Supporting Information

Real-Time Single-Molecule Observation of a Chemical Reaction Reshaping the Energy Landscape of a Molecular Shuttle

Tomás Nicolás-García,[a] Natalia Martín Sabanés,[a] Rebeca Bocanegra,[a] Gloria Tobajas-Curiel,[a] Borja Ibarra,*[a] and Emilio M. Pérez*[a]

[a] Dr. T. Nicolás-García, Dr. N. Martín Sabanés, Dr. R. Bocanegra, Dr. G. Tobajas-Curiel, Dr. B. Ibarra, Prof. Dr. E. M. Pérez
IMDEA Nanociencia
C/ Faraday 9, Campus de Cantoblanco, 28049 Madrid (Spain)
E-mail: borja.ibarra@imdea.org, emilo.perez@imdea.org

Table of Contents

SUPPORTING INFORMATION

S1. General synthetic methodology

All solvents were dried according to standard procedures. Reagents were used as purchased. All air-sensitive reactions were carried out under inert atmosphere. DNA oligonucleotides were purchased from Biomers. Column chromatography was carried out using silica gel (Merck, Kieselgel 60, 230-240 mesh) as a stationary phase. Analytical thin layer chromatography (TLC) was performed on precoated silica gel on aluminum cards (0.25 mm thick, with fluorescent indicator 254 nm) and observed under UV light. NMR spectra were recorded on a BrukerAvance 400 (^{1}H: 400 MHz; ^{13}C: 101 MHz) spectrometer at 298 K, unless otherwise stated. Residual solvent signals were used as internal references. In $CDCl_3$ ^{1}H and ^{13}C spectra were referenced to δ 7.26 ppm and δ 77.06 ppm, respectively. In DMSO-d_6, spectra were referenced to δ 2.50 ppm (^{1}H) and δ 39.52 ppm (^{13}C). In D_2O, ^{1}H spectra were referenced to δ 4.79 ppm. Spectra of the synthesized compounds were assigned with the aid of both DEPT and 2D NMR experiments (COSY, HMQC or HMBC). Coupling constants (*J*) are expressed in Hz and chemical shifts (δ) in ppm. Multiplicities are denoted as follows: s = singlet; br = broad; d = doublet; t = triplet; m = multiplet. High-Resolution Mass Spectroscopy (HRMS) was obtained using both Atmospheric-Pressure Chemical Ionization (APCI) and Electrospray Ionization (ESI) on a MAXIS II (Bruker) spectrometer, Matrix-Assisted Laser Desorption Ionization (MALDI-TOF) on a VS AutoSpec spectrometer, both coupled to a time-of-flight (TOF) instrument and time-of-flight mass spectrometry coupled to a Gas Chromatograph with Electron Ionization (GCEI) on a GCT Agilent Technologies 6890N. UV-Vis spectroscopy was performed on a Cary 50 UV-Visible spectrophotometer. Fourier-transform infrared spectroscopy with attenuated total reflection (FT-ATR-IR) was performed on a Bruker ALPHA FTIR spectrometer. The conditions used for all the data collected were: 24 scans, 24 seconds each experiment, transmission mode.

Abbreviation list:

BHMF: 2,5-Bis(hydroxymethyl)furan

DBU: Diazabicycloundecene

DCM: Dichloromethane

DMAP: 4-Dimethylaminopyridine

DMF: *N,N*-dimethylformamide

EDCI·HCl: *N*-(3-dimethylaminopropyl)-*N*'-ethylcarbodiimide hydrochloride

PEG: Polyethylene glycol

TFA: Trifluoroacetic acid

THF: Tetrahydrofuran

TLC: Thin Layer Chromatography

WLC: Worm-like chain (model)

S2. Synthesis of molecular shuttle 15

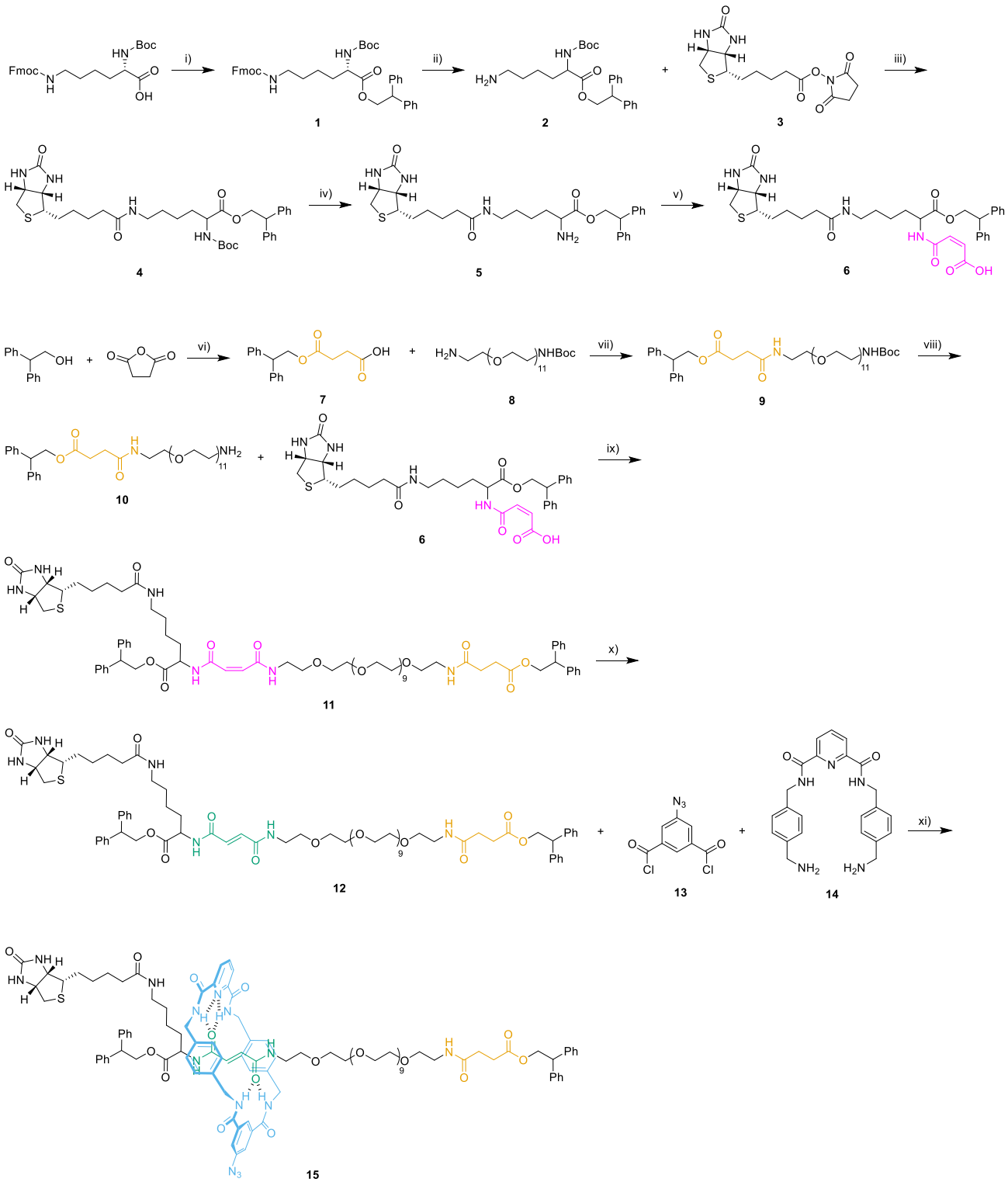

Figure S2.1. Preparation of molecular shuttle **15**. Reagents and conditions: i) 2,2-diphenylethanol, DMAP, EDCI·HCl, DCM, 0 ºC to r.t. 12 h, 99%; ii) piperidine, DBU, DMF, r.t. 4 h, 99%; iii) Et_3N, DMF, 0 ºC to r.t. 12 h, 96%; iv) TFA, DCM, 0 ºC to r.t. 4 h, 99%; v) maleic anhydride, Et_3N, THF, 0 ºC to r.t. 12 h, 90%; vi) Et_3N, DCM, 12 h, 76%; vii) EDCI·HCl, DMAP, DCM, 0 ºC to r.t. 12 h, 90%; viii) TFA, DCM, 0 ºC to r.t. 4 h, 99%; ix) EDCI·HCl, DMAP, DCM, 0 ºC to r.t. 12 h, 60%; x) Piperidine, DCM, 48 h, 97%; xi) Et_3N, $CHCl_3$, r.t. 12 h, 46%.

SUPPORTING INFORMATION

Compound 1

To a solution of Boc-D-Lys(Fmoc)-OH (900 mg, 1.92 mmol) in dry DCM (25 mL) under N_2 atmosphere, diphenylethanol (457 mg, 2.3 mmol) and a catalytic amount of DMAP were added and the mixture was stirred at 0 ºC for 5 minutes. Afterwards, EDCI·HCl (732 mg, 3.84 mmol) was added at 0 ºC and the reaction mixture was stirred at room temperature overnight. The reaction mixture was concentrated under reduced pressure and then diluted with DCM. Next, the mixture was washed with 1 M HCl (2 x 100 mL), $NaHCO_3$ (sat. aq.) (2 x 100 mL) and brine (1 x 100 mL). The organic layers were dried over anhydrous $MgSO_4$ and concentrated under reduced pressure. The crude was purified by column chromatography on silica gel using a hexane/EtOAc 75/25 mixture as eluent, to furnish compound **1** as colorless oil (1.12 g, 99%). Its spectroscopic data were in concordance with those described in bibliography.[1]

Compound 2

Compound **1** (90 mg, 0.14 mmol) was dissolved in 1% piperidine and 1% DBU in DMF (2.8 mL). The reaction mixture was stirred for 3 hours at room temperature until the Fmoc deprotection was completed (followed by TLC). The solvent was removed under reduced pressure to give compound **2** as yellowish oil (assumed quantitative yield) and the crude material was used in the next step reaction without further purification. Its spectroscopic data were in concordance with those described in bibliography.[1]

Compound 3

EDCI·HCl (71 mg, 0.37 mmol) was added to a solution of D-biotin (75 mg, 0.31 mmol) and *N*-hydroxysuccinimide (39 mg, 0.34 mmol) in DMF at 0 ºC. The reaction mixture was stirred at room temperature for 24 hours. Afterwards, solvent was removed to obtain a solid. Finally, the solid was washed several times with methanol to furnish compound **3** as a white solid (96 mg, 90%). Its spectroscopic data were in concordance with those described in bibliography.[1]

Compound 4

Compounds **2** (46 mg, 0.110 mmol), **3** (25 mg, 0.073 mmol), and 2 drops of Et_3N were dissolved in DMF (5 mL) and the reaction mixture was stirred overnight. Afterwards, the residue was diluted in DCM and washed by water. The organic phase was dried over anhydrous $MgSO_4$ and concentrated under reduced pressure. The crude was purified by column chromatography on silica gel using a gradient elution, from $CHCl_3$ to $CHCl_3$/MeOH 90/10, to furnish compound **4** as colorless oil (45 mg, 96%). Its spectroscopic data were in concordance with those described in bibliography.[1]

Compound 5

To a solution of compound **4** (120 mg, 0.19 mmol) in DCM (2 mL) TFA (0.30 mL, 4.00 mmol) was added dropwise at 0 ºC. The reaction was stirred at room temperature for 4 hours until it was completed (followed by TLC). Then, the solvent and excess of TFA were removed under reduced pressure and the crude was dissolved in a mixture DCM/MeOH 1/1 and Amberlyst® A21 was added. The mixture was stirred at room temperature for 1 hour. Afterwards, the mixture was filtered off, and the solvent was

removed under reduced pressure, to furnish the unprotected amine **5**, which was used in the next step without further purification. Its spectroscopic data were in concordance with those described in bibliography.[1]

Compound 6

Compound **5** (49 mg, 0.09 mmol) and 1 drop of Et_3N were dissolved in dry THF (1 mL) at 0 ºC, then maleic anhydride (9 mg, 0.093 mmol) dissolved in dry THF (0.4 mL) was dropwise added under inert atmosphere and the mixture was stirred at room temperature overnight. Afterwards, the solvent was removed under reduced pressure. The crude was purified by column chromatography on silica gel using a gradient elution, from DCM to DCM/MeOH 90/10 to DCM/MeOH/NH_3 80/20/0.2, to furnish compound **6** as yellowish oil (59 mg, 90%). Its spectroscopic data were in concordance with those described in bibliography.[1]

Compound 7

2,2-diphenylethanol (1 g, 5.26 mmol) and 1 drop of Et_3N were dissolved in dry DCM (53 mL) and a solution of succinic anhydride (584 mg, 5.83 mmol) in DCM (15 mL) was added dropwise for 30 minutes and the mixture was stirred at room temperature overnight. Afterwards, the solvent was removed under reduced pressure. The crude was purified by column chromatography on silica gel using a hexane/EtOAc 70/30 mixture as eluent, to furnish the compound **7** as white solid (1.2 g, 76%). Its spectroscopic data were in concordance with those described in bibliography.[1]

Compound 9

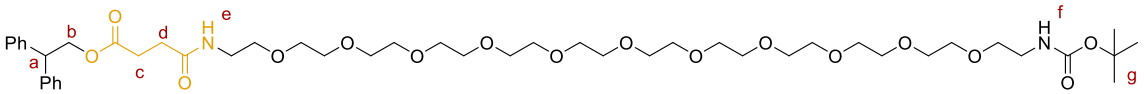

To a suspension of carboxylic acid **7** (57 mg, 0.19 mmol) under N_2 atmosphere, commercially sourced O-(2-aminoethyl)-O′-[2-(Boc-amino)ethyl]decaethylene glycol (**8**, 100 mg, 0.15 mmol) and DMAP (25 mg, 0.20 mmol) were added, and the solution was stirred at 0 ºC for 10 minutes. Afterwards, EDCI·HCl (40 mg, 0.20 mmol) was added at 0 ºC and the reaction was stirred at room temperature for 24 hours. Next, the mixture was washed with 1 M HCl (2 x 100 mL), $NaHCO_3$ (sat. aq.) (2 x 100 mL) and brine (1 x 100 mL). The organic phases were dried over anhydrous $MgSO_4$ and concentrated under reduced pressure. The crude was purified by column chromatography on silica gel using a $CHCl_3$/MeOH 95/5 mixture as eluent, to furnish compound **9** as yellowish oil (125 mg, 90%).

^{1}H NMR (400 MHz, $CDCl_3$, 298 K) δ = 7.34 – 7.14 (m, 10H, Ar-H), 6.33 (br, 1H, NH_e), 5.11 (br, 1H, NH_f), 4.62 (d, *J* = 7.6 Hz, 2H, H_b), 4.35 (t, *J* = 7.6 Hz, 1H, H_a), 3.63 (m, *J* = 5.6 Hz, 40H, PEG-H), 3.51 (m, 4H, PEG-H), 3.40 (m, 2H, PEG-H), 3.30 (m, 2H, PEG-H), 2.56 (t, *J* = 7.0 Hz, 2H, H_c), 2.37 (t, *J* = 7.0 Hz, 2H, H_d), 1.44 (s, 9H, H_g).

^{13}C NMR (100 MHz, $CDCl_3$, 298 K) δ = 172.7 (C=O), 171.3 (C=O), 156.0 (C=O), 141.1 (C), 128.6 (CH), 128.2 (CH), 126.8 (CH), 79.1 (CH_2), 70.6 (CH_2), 70.2 (CH_2), 69.8 (CH_2), 66.8 (CH_2), 49.8 (CH), 40.4 (CH_2), 39.3 (CH_2), 30.7 (CH_2), 29.5 (CH_2), 28.5 (CH).

HRMS (APCI) calculated for $C_{47}H_{77}N_2O_{16}$ $[M+H]^+$ 925.5268, found 925.5244.

Compound 10

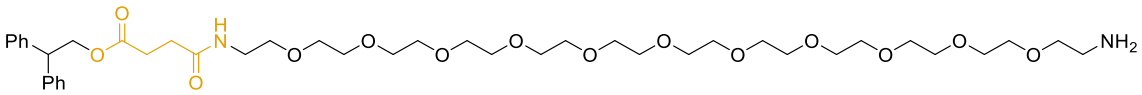

To a solution of compound **9** (110 mg, 0.12 mmol) in DCM (2 mL) TFA (0.30 mL, 4.00 mmol) was added dropwise at 0 ºC. The reaction was stirred at room temperature for 4 hours until it was completed (followed by TLC). Then, the solvent and excess of TFA were removed under reduced pressure and the crude was dissolved in a mixture DCM/MeOH 1/1 and Amberlyst® A21 was added. The mixture was stirred at room temperature for 1 hour. Afterwards, the resin was filtered, and the solvent was removed under reduced pressure, to furnish the unprotected amine **10**, which was used in the next step without further purification.

Thread 11

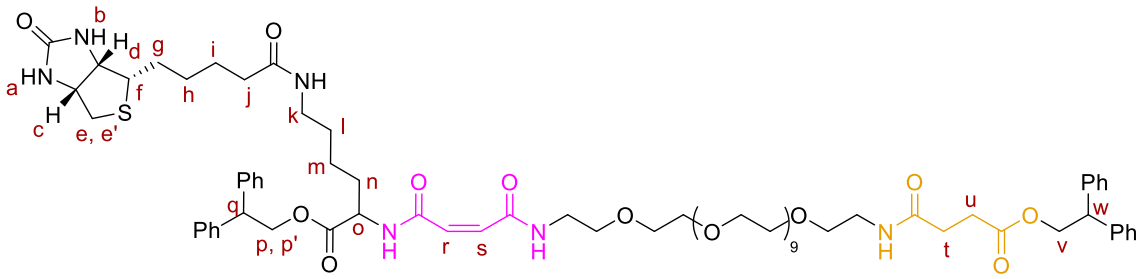

To a suspension of carboxylic acid **6** (85 mg, 0.13 mmol) in dry DCM (10 mL) under N_2 atmosphere, the amine **10** (107 mg, 0.12 mmol) and DMAP (23 mg, 0.19 mmol) were added, and the solution was stirred at 0 ºC for 5 minutes. Afterwards, EDCI·HCl (37 mg, 0.19 mmol) was added at 0 ºC and the reaction was stirred at room temperature for 24 hours. Next, the mixture was washed with 1 M HCl (2 x 100 mL), $NaHCO_3$ (sat. aq.) (2 x 100 mL) and brine (1 x 100 mL). The organic phase was dried over anhydrous $MgSO_4$ and concentrated under reduced pressure. The crude was purified by column chromatography on silica gel using a gradient elution, from DCM/MeOH 95/5 to 90/10, to furnish (*Z*/*E* 55/45)-thread **11** as colourless oil (112 mg, 60%).

^{1}H NMR (400 MHz, DMSO-*d*$_6$, 298 K) δ = 9.79 (d, *J* = 7.0 Hz, 0.5H, NH-*Z*-isomer), 9.06 (t, *J* = 5.6 Hz, 0.5H, NH-*Z*-isomer), 8.66 (d, *J* = 7.1 Hz, 0.5H, NH-*E*-isomer), 8.50 (t, *J* = 5.7 Hz, 0.5H, NH-*E*-isomer), 7.87 (t, *J* = 5.6 Hz, 1H, NH), 7.70 (m, *J* = 4.7 Hz, 1H, NH), 7.41 – 7.24 (m, 16H, Ar), 7.26 – 7.13 (m, 4H, Ar), 6.87 (d, *J* = 15.2 Hz, 0.4 H, H_r or H_s of *E*-isomer), 6.82 (d, *J* = 15.2 Hz, 0.4 H, H_r or H_s of *E*-isomer), 6.41 (br, 1 H, H_a), 6.34 (br, 1 H, H_b), 6.21 (d, *J* = 13.1 Hz, 0.5 H, H_r or H_s of *Z*-isomer), 6.07 (d, *J* = 13.1 Hz, 0.5 H, H_r or H_s of *Z*-isomer), 4.73 (dd, *J* = 10.7, 8.2 Hz, 1H, H_p or $H_{p'}$), 4.56 (m, 3H, $H_{p'}$ or H_p, H_v), 4.43 – 4.22 (m, 3H, H_c, H_q, H_w), 4.12 (m, 2H, H_d, H_o), 3.50 (m, 44H, PEG-H), 3.37 (t, *J* = 5.9 Hz, 2H, PEG-H), 3.16 (dd, *J* = 11.5, 5.8, Hz, 2H, PEG-H), 3.08 (m, 1H, H_f), 2.91 (m, 2H, H_k), 2.81 (dd, *J* = 12.4, 5.1 Hz, 1H, H_e or $H_{e'}$), 2.60 (d, J = 14.1 Hz, 1 H, He´ or He), 2.37 (t, *J* = 7.0 Hz, 2H, H_u), 2.27 (t, *J* = 6.7 Hz, 2H, H_t), 2.04 (t, *J* = 7.4 Hz, 2H, H_j), 1.68 – 1.09 (m, 12H, $H_{g+h+i+l+m+n}$).

^{13}C NMR (100 MHz, DMSO-*d*$_6$, 298 K) δ = 172.3 (C=O), 171.8 (C=O), 171.5 (C=O), 170.6 (C=O), 162.7 (C=O), 141.5 (C), 141.3 (C), 141.2 (C), 128.5 (CH), 128.0 (CH), 126.6 (CH), 69.8 (CH_2), 69.6 (CH_2), 69.1 (CH_2), 66.4 (CH_2),66.0 (CH_2), 61.0 (CH), 59.2 (CH), 55.4 (CH), 49.2 (CH_2), 35.2 (CH_2), 29.6 (CH_2), 28.9 (CH_2), 28.8 (CH_2), 28.2 (CH_2), 28.0 (CH_2), 25.3 (CH_2).

HRMS (APCI) calculated for $C_{76}H_{109}N_6O_{20}S$ $[M+H]^+$ 1457.7412, found 1457.7401.

Thread 12

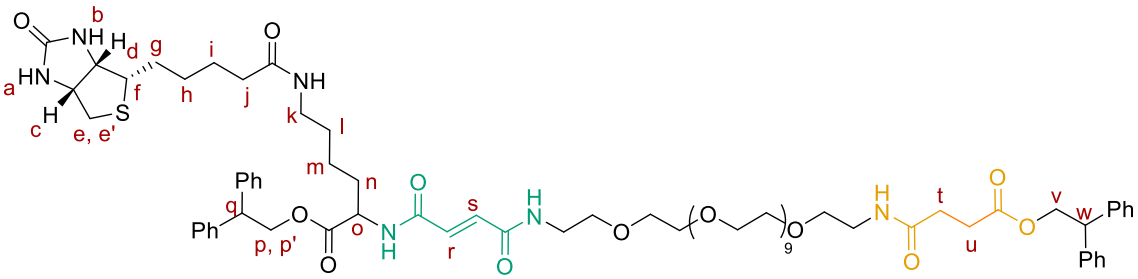

A solution of **11** (63 mg, 0.043 mmol) and 3 drops of piperidine in dry DCM (3 mL) was stirred at room temperature for 48 hours. Then, DCM was added, and the organic layer was washed twice with HCl 1 M and dried over anhydrous $MgSO_4$ and concentrated under reduced pressure to furnish thread **12** as yellowish oil (61 mg, 97%).

^{1}H NMR (400 MHz, DMSO-*d*$_6$, 298 K) δ = 8.66 (d, *J* = 7.2 Hz, 1H, NH), 8.51 (t, *J* = 5.7 Hz, 1H, NH), 7.87 (t, *J* = 5.5 Hz, 1H, NH), 7.71 (t, *J* = 5.3 Hz, 1H NH), 7.38 – 7.27 (m, 16H), 7.21 (m, 4H), 6.87 (d, *J* = 15.3 Hz, 1H, H_r or H_s), 6.82 (d, *J* = 15.3 Hz, 1H, H_s or H_r), 6.41 (br, 1H, H_a), 6.34 (br, 1H, H_b), 4.72 (dd, *J* = 10.9, 8.1 Hz, 1H, H_p or $H_{p'}$), 4.55 (m, 3H, $H_{p'}$ or H_p, H_v), 4.33 (m, 3H, H_c, H_q, H_w), 4.13 (m, 2H, H_d, H_o), 3.58 – 3.42 (m, 44H, PEG-H), 3.37 (t, *J* = 5.9 Hz, 2H, PEG-H), 3.17 (dd, *J* = 11.5, 5.9 Hz, 2H, PEG-H), 3.09 (m, 1H, H_f), 2.91 (m, 2H, H_k), 2.81 (dd, *J* =12.4, 5.1 Hz, 1H, H_e or $H_{e'}$), 2.57 (d, *J* = 12.4 Hz, 1H, $H_{e'}$ or H_e), 2.37 (t, *J* = 6.8 Hz, 2H, H_u), 2.27 (t, *J* = 6.8 Hz, 2H, H_t), 2.04 (t, *J* = 6.8 Hz, 2H, H_j), 1.68 – 1.09 (m, 12H, $H_{g+h+i+l+m+n}$).

^{13}C NMR (100 MHz, DMSO-d_6, 298 K) δ = 172.3 (C=O), 171.8 (C=O), 171.6 (C=O), 170.6 (C=O), 163.8 (C=O), 163.7 (C=O), 162.7 (C=O), 141.5 (C), 141.3 (C), 141.2 (C), 128.5 (CH), 127.9 (CH), 126.6 (CH), 69.8 (CH_2), 69.6 (CH_2), 69.1 (CH_2), 68.9 (CH_2), 66.4 (CH_2), 66.0 (CH_2), 61.0 (CH), 59.2 (CH), 55.4 (CH), 52.3 (CH_2), 49.2 (CH_2), 35.2 (CH_2), 30.3 (CH_2), 29.6 (CH_2), 28.9 (CH_2), 28.8 (CH_2), 28.2 (CH_2), 28.0 (CH_2), 25.3 (CH_2), 22.6 (CH_2).

HRMS (APCI) calculated for $C_{76}H_{109}N_6O_{20}S$ $[M+H]^+$ 1457.7412, found 1457.7428.

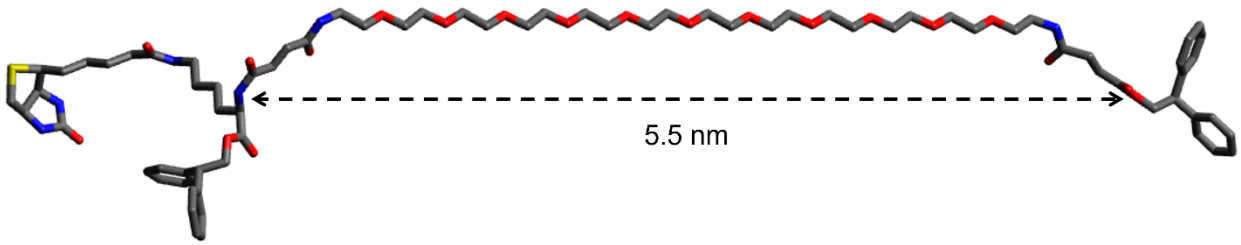

Figure S2.2. DFT calculations determined 5.5 nm between the N terminal atom of the fumaramide station (green) and the O terminal atom of the succinic amide-ester station (orange) in thread **12**.

Compound 13

5-aminoisophalic acid (2.5 g, 27.6 mmol) was dissolved in water (39 mL) at 0 ºC and 3 mL of 12 M HCl was added dropwise. $NaNO_2$ was then dissolved in water and added dropwise to the mixture, which was stirred for 30 min. Afterwards, NaN_3 was also dissolved in water and added dropwise to the mixture. A yellow solid was formed, and gas evolution was observed. The mixture was stirred until gas evolution was no longer detected. The product was then filtered off, washed with distilled water, and dried under vacuum to get 5-azido-isophthalic acid (3.4 g, 60%). Next, oxalyl chloride (0.15 mL, 1.95 mmol) was added to a stirred suspension of 5-azido-isophthalic acid (100 mg, 0.48 mmol) and 2 drops of DMF in DCM (2 mL). The reaction mixture was stirred until the product was totally solubilized. The solvent was then removed under reduced pressure, and the crude was kept under vacuum for 3 hours to remove the excess oxalyl chloride. The crude product was used directly in the next step without further purification. Its spectroscopic data were in concordance with those described in bibliography.[1]

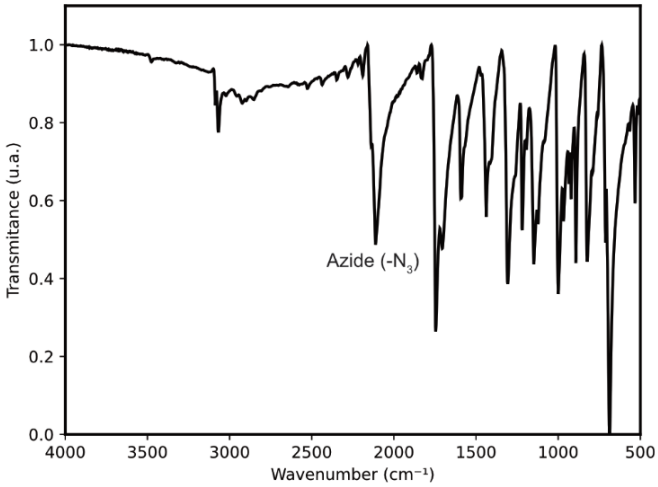

Figure S2.3. ATR-FTIR of compound **13**. Band from azide group ($-N_3$) appears at 2111 cm^{-1}.

Compound 14

To a solution of *p*-xylylenediamine (515 mg, 3.78 mmol) in $CHCl_3$ (60 mL) at 0 ºC, a solution of Boc_2O (413 mg, 1.89 mmol) in $CHCl_3$ (45 mL) was added dropwise over a period of 4 hours. The mixture was stirred at room temperature overnight under an inert atmosphere. The resulting solid was filtered and washed with cold $CHCl_3$. Next, solvent was removed under reduced pressure, and DCM and water were added to the remaining oil. The layers were separated, and the aqueous layer was extracted with DCM. The organic phase was dried over anhydrous $MgSO_4$ and concentrated under reduced pressure. The crude was purified by column chromatography on silica gel using a gradient elution, from DCM/MeOH 95/5 to 85/15 to give *N*-Boc-4-(aminomethyl)benzylamine (400 mg, 90%). On the other hand, 2,6-pyridinedicarboxylic acid (234 mg, 1.4 mmol) and 2 drops of DMF were dissolved in dry DCM at 0 ºC, then oxalyl chloride was added dropwise. The reaction mixture was stirred until the product was totally solubilized. The solvent was then removed, and the crude solid was dried under high vacuum for 2 hours. The acid chloride formed was dissolved in $CHCl_3$ and added dropwise to a solution of the previously synthetized *N*-Boc-4-(aminomethyl)benzylamine, and Et_3N in $CHCl_3$. The reaction mixture was stirred overnight. Afterwards, the solvent was removed under reduced pressure, and the remaining oil was dissolved in DCM and washed with water. The organic phase was dried over anhydrous $MgSO_4$ and concentrated under reduced pressure. The crude was purified by column chromatography on silica gel using a gradient elution, from DCM/MeOH 95/5 to 85/15 to give the Boc-protected precursor (400 mg, 90%). Finally, the Boc-protected precursor was dissolved in DCM at 0 ºC and TFA (0.30 mL, 4.00 mmol) was added dropwise at 0 ºC. The reaction was stirred at room temperature for 4 hours until it was completed (followed by TLC). Then, the solvent and excess of TFA were removed under reduced pressure and the crude was dissolved in a mixture DCM/MeOH 1/1 and Amberlyst® A21 was added. The mixture was stirred at room temperature for 1 hour. Afterwards, the resin was filtered, and the solvent was removed under reduced pressure, to furnish the unprotected amine **19**, which was used in the next step without further purification. Its spectroscopic data were in concordance with those described in bibliography.[1]

Molecular shuttle 15

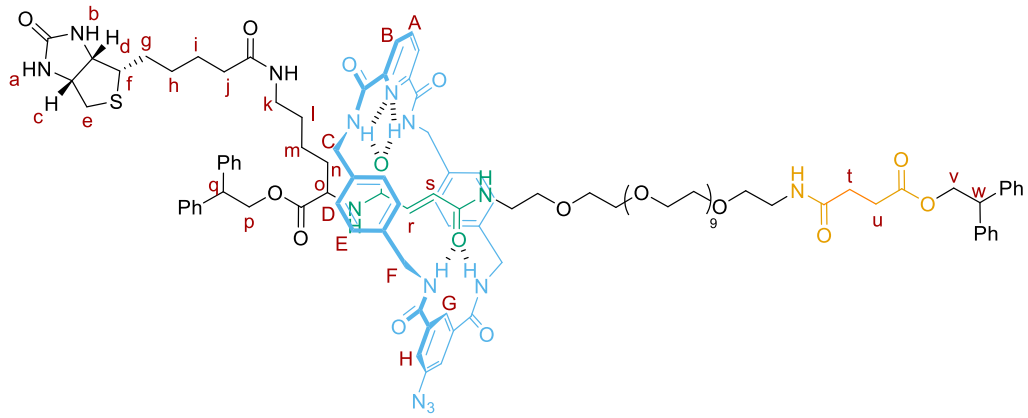

Thread **12** (30 mg, 0.02 mmol) and Et_3N (0.1 mL, 0.72 mmol) were dissolved in 4 mL $CHCl_3$ (stabilized with amylenes). The mixture was stirred vigorously whilst solutions of the diamine **14** (100 mg, 0.25 mmol) in $CHCl_3$ (3 mL) and the acid chloride **13** (61 mg, 0.25 mmol) in $CHCl_3$ (3 mL) were simultaneously added over a period of 3 hours using motor-driven syringe pumps. After 12 hours, the solvent was removed under reduced pressure and the resulting residue was purified by column chromatography on silica gel using a DCM/MeOH 92/8 mixture as eluent, to furnish the rotaxane **15** as colourless oil (15 mg, 46%).

^{1}H NMR (400 MHz, DMSO-d_6, 298 K) δ = 9.60 (m, 2H, NH), 8.74 (d, J = 6.8 Hz, 1H, NH), 8.53 (t, J = 5.6 Hz, 1H, NH), 8.34 (m, 1H, H_A), 8.23 (m, 2H, H_B), 7.91 (t, J = 4.6 Hz, 1H, NH), 7.84 (m, 2H, NH), 7.71 (t, J = 5.5 Hz, 1H, NH), 7.22 (m, 23H, H_{G+H+Ar}), 7.08 (m, 8H, H_{D+E}), 6.40 (br, 1H, H_a), 6.34 (br, 1H, H_b), 6.21 (m, 2H, H_{r+s}), 4.72 (dd, J = 10.9, 8.5 Hz, 1H, H_p or $H_{p'}$), 4.54 (m, 7H, $H_{p'}$ or H_p, H_v and H_C or H_F), 4.45 – 4.22 (m, 7H, H_c, H_q, H_w and H_C or H_F), 4.11 (m, 2H, H_d, H_o), 3.50 (m, 2H, PEG-H), 3.40 (m, 12H, PEG-H), 3.30 (m, 28H, PEG-H), 3.20 (m, 2H, PEG-H), 3.09 (m, 5H, PEG-H and H_f), 2.93 (m, 2H, H_k), 2.80 (dd, J =12.4, 5.1 Hz, 1H, H_e or $H_{e'}$), 2.57 (d, J = 12.4 Hz, 1H, $H_{e'}$ or H_e), 2.28 (t, J = 7.0 Hz, 2H, H_u), 2.16 (t, J = 7.0 Hz, 2H, H_t), 2.04 (t, J = 7.4 Hz, 2H, H_j), 1.48 (m, 12H, $H_{g+h+i+l+m+n}$).

HRMS (ESI) calculated for $C_{107}H_{134}N_{14}O_{24}SNa$ $[M+Na]^+$ 2053.9308, found 2053.9285.

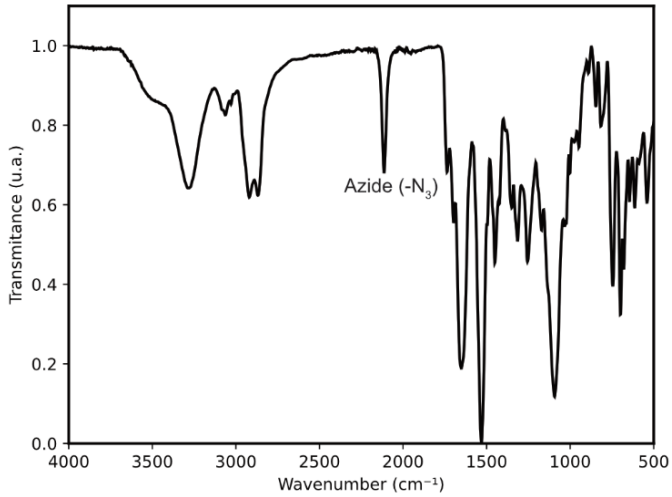

Figure S2.4. ATR-FTIR of molecular shuttle **15**. Band from azide group ($-N_3$) appears at 2115 cm^{-1}.

A ^{1}H NMR spectrum comparison between the thread **12** (**Figure S2.5a**) and the molecular shuttle **15** (**Figure S2.5b**) was performed to corroborate its interlocked nature.

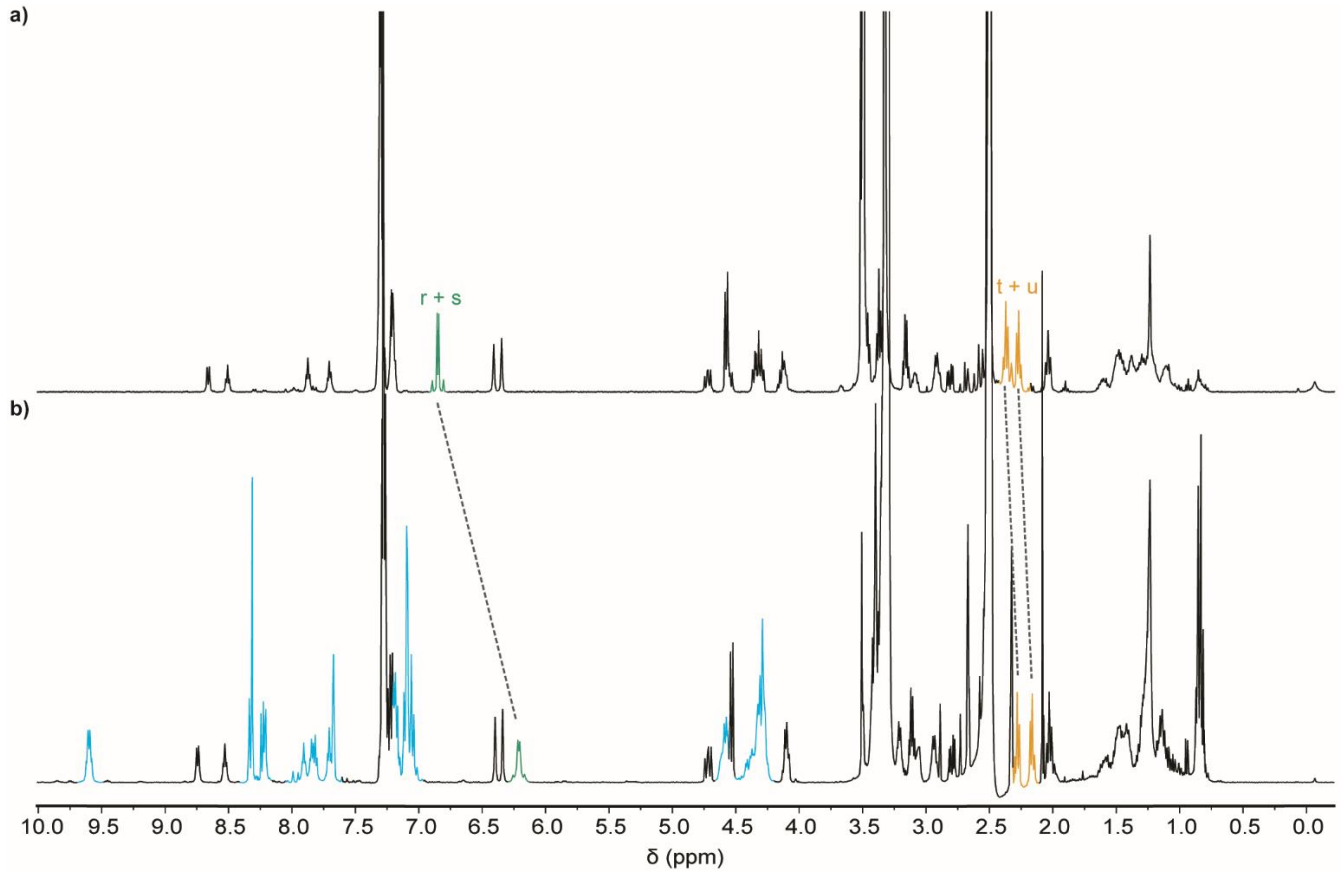

Figure S2.5. ^{1}H NMR spectra (400 MHz, DMSO-d_6, 298 K) of **a)** thread **12**; **b)** molecular shuttle **15**. The molecular shift displacement of fumaramide signals (*fum*, in green) and succinic amide-ester signals (*succ*, in orange) is due to the different diamagnetic shielding effect of the macrocycle over both stations. The higher displacement in the *fum* signals means the macrocycle (in blue) spends more time over it under these experimental conditions.

Molecular shuttle-dsDNA hybrid 19

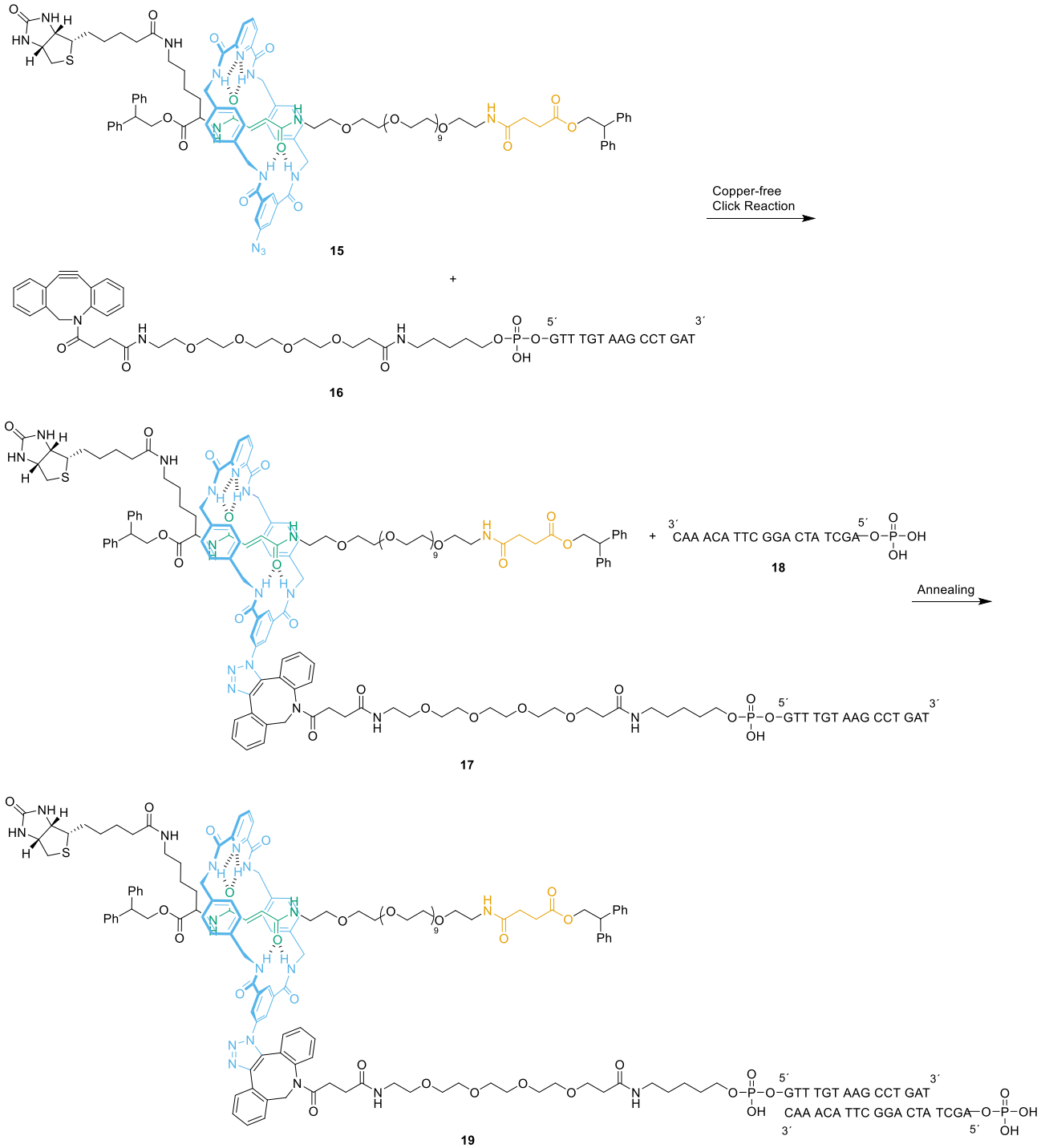

Figure S2.5. Preparation of the molecular shuttle-dsDNA hybrid **19**.

100 µM solutions of molecular shuttle **15** in DMF (75 µL) and ssDNA **16** (DBCO-PEG4-GTTTGTAAGCCTGAT) in water (35 µL) were mixed and 100 µL of Milli-Q® water was added to a final volume of 210 µL. The mixture was stirred at room temperature overnight. Afterwards, the solvent was eliminated in a SpeedVac™ vacuum concentrator and the molecular shuttle-ssDNA hybrid **17** was subsequently resuspended in 70 µL of Milli-Q® water. Next, 50 µM aqueous solutions of molecular shuttle-ssDNA hybrid **17** (2 µL) and 100 µM oligonucleotide **18** (Phos-AGCTATCAGGCTTACAAAC) (1

µL) were mixed in 40 µL final volume of annealing buffer (20 mM Tris-HCl, 100 mM NaCl, 2 mM EDTA). The final mixture was incubated at 95 ºC for 5 minutes and then it was allowed to cool to 25 ºC gradually. In this way, the molecular shuttle-dsDNA hybrid **19** which contains the molecular shuttle at its end was prepared. In the opposite end, the annealed dsDNA holds a protruding AGCT 5' end, compatible with the 5' protruding end produced in a HindIII digestion.

S3. Coupling of the molecular shuttle-dsDNA hybrid 19 to DNA handles

The molecular shuttle was connected between two functionalized beads using two dsDNA handles for optical tweezers experiments. The shorter 837 bp dsDNA handle that will connect the thread of the molecular shuttle to the micropipette-bead via streptavidin-biotin attachment was synthetized by PCR amplification of a section of the pUC19 vector with two DNA oligonucleotides: one labelled with biotin and the other with digoxigenin at the 5′-end. The handle was then incubated with saturating amounts of streptavidin and attached to anti-digoxigenin covered polystyrene micron-beads (Spherotech, Co). One of these beads is held by suction on top of a micropipette in the microfluidics chamber.

On the other hand, the longer 2701 bp dsDNA handle connects the macrocycle to the bead in the optical trap. This handle was obtained from the pUC19 vector (Novagen) using restriction digestion with BamHI and HindIII endonucleases. In a single step, the digestion result was ligated at the BamHI end with a DNA segment labelled with numerous digoxigenin units,[2] and at the HindIII end with molecular shuttle-dsDNA hybrid **19**, which has 15 additional base pairs.

The final molecular shuttle-dsDNA hybrid was then linked to anti-digoxigenin-coated beads (Spherotech Co.) and these diluted in the measurement buffer before being flowed into the fluidic chamber, where they can be manipulated using the optical trap. Single molecular shuttle-dsDNA hybrids must be tethered after attaching the molecular shuttle's biotin end to the streptavidin unit at the extreme of the 837 bp dsDNA handle, which is in turn linked to the pipette-bead.

S4. Optical tweezers experiments

Optical tweezers measurements were performed at 22 ± 1 °C with a highly stable miniaturized dual-beam optical tweezers,[3] with a limiting spatial resolution of ≤ 1 nm.

Pulling-relaxing cycles were recorded at a constant pulling rate of 200 nm s^{-1}. The setup controls the distance between the trap center and the micropipette tip (X_{total}), which differs from the end-to-end distance of the molecular system under consideration ($X_{end-end}$). The system's end-to-end distance is computed by the following formula:

$$X_{end-end} = X_{total} - \frac{F}{k}$$

where F is the force applied to the system, k the stiffness of the trap, and $\frac{F}{k}$ corresponds to the distance traversed (in nm) by the bead out of the trap center (bead position). We assume a linear spring restoring force. The stiffness of the trap depends on the power of the lasers, the size and refractive index of the bead in the trap as well as the viscosity of the surrounding medium. In our experimental conditions, for the 3 μm diameter beads employed and a laser power of 60 mW, the value of the stiffness is k = 0.135 ± 0.004 pN nm^{-1}. A feedback stabilized protocol was used for constant force measurements, that maintain them within ~0.05 pN by moving the beads closer or further apart. All experimental data was recorded at 0.5 kHz.

In our dual-beam optical tweezers operating at 830 nm, laser-induced heating of the aqueous medium is expected to be very small under the trapping conditions used here. The trap is formed by two counter-propagating beams of 60 mW each, and previous estimates for comparable instruments indicate only a modest temperature rise at the focus.[4-6] In addition, because the molecular shuttle is located away from the trapped bead through the dsDNA handle, the local temperature increase at the position of the molecule is expected to be smaller than that at the laser focus.[4] We therefore consider the corresponding variation in k_BT as well as in the Brownian fluctuations of the macrocycle to be negligible within the precision of the present experiments, and no explicit temperature correction was applied in the analysis.

In this work, individual molecular shuttles were examined at the single-molecule level. For this purpose, an optically trapped bead functionalized with a molecular shuttle was brought into close proximity to a second bead held by a micropipette tip, enabling a specific biotin-streptavidin interaction. This interaction tethered the molecular shuttle-dsDNA hybrid in an end-to-end configuration within the experimental setup. Each molecular construct was then subjected to repeated pulling-relaxing cycles. The resulting force-extension curves were well described by the worm-like chain (WLC) model, yielding a persistence length of 50 nm, in agreement with established values for dsDNA and thereby confirming single-molecule conditions (see **Section S6**).

After confirming single-molecule conditions, hopping experiments were performed using a force-feedback protocol, in which various constant forces were applied until the end-to-end attachments ruptured. The tracking of these chemical stimulation experiments at this molecular scale are inherently challenging, as the system may fail due to environmental mechanical perturbations or excessive forces that compromise the anchoring points. From the full set of acquired hopping traces, only those of sufficient duration for quantitative analysis were selected for this study. The raw hopping traces were baseline-corrected by fitting a polynomial function of order 1 to 3, depending on the trace. Traces that could not be adequately described by a polynomial fit were considered unstable and were excluded from the analysis. The baseline-correction algorithm, developed in MATLAB, is available at: https://hdl.handle.net/20.500.12614/3812.

S5. Test of the Diels-Alder reaction in aqueous medium with molecular shuttle model 23

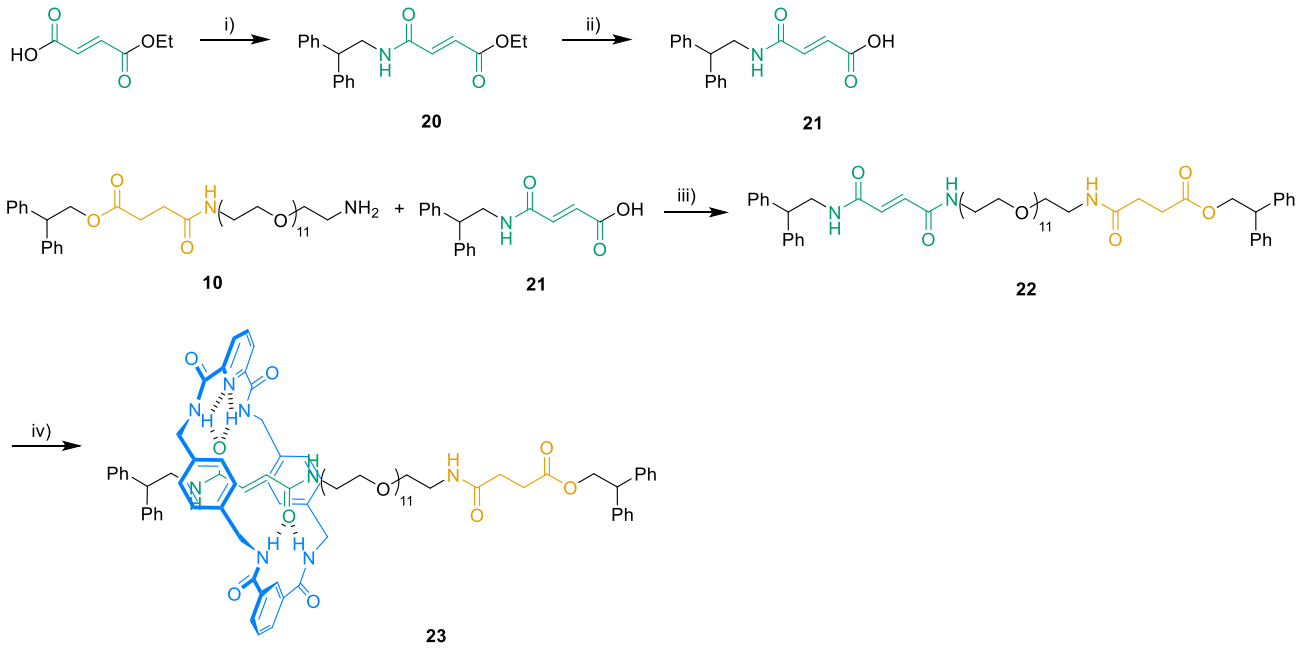

Figure S5.1 Preparation of molecular shuttle model **23**: i) 2,2-diphenylethylamine, 4-DMAP, EDCI·HCl, DCM, 0 ºC to r.t. 24 h, 77%; ii) KOH, EtOH, r.t. 24 h, 90%; iii) 4-DMAP, EDCI·HCl, DCM, 0 ºC to r.t. 24 h, 40%. iv) isophthaloyl dichloride, **14**, Et_3N, $CHCl_3$, r.t. 12 h, 29%.

Compound 20

To a solution of (*E*)-4-ethoxy-4-oxobut-2-enoic acid (3.32 g, 23.03 mmol) in dry DCM (150 mL) under N_2 atmosphere, 2,2-diphenylethylamine (5.00 g, 25.33 mmol) and DMAP (2.81 g, 23.03 mmol) were added, and the solution was stirred at 0 ºC for 10 minutes. Afterwards, EDCI·HCl (4.42 g, 23.03 mmol) was added at 0 ºC and the reaction was stirred at room temperature for 24 hours. Then, the mixture was washed with 1 M HCl (2 x 100 mL), $NaHCO_3$ (sat. aq.) (2 x 100 mL) and brine (1 x 100 mL). The organic phase was dried over anhydrous $MgSO_4$ and concentrated under reduced pressure to furnish the compound **20** as a white solid (5.70 g, 77%). Its spectroscopic data were in concordance with those described in bibliography.[7]

Compound 21

To a solution of ester **20** (5.18 g, 16.04 mmol) in absolute EtOH (100 mL) an aqueous solution of KOH (1.86 g, 33.20 mmol) in 12.4 mL of water was added. The mixture was stirred at room temperature overnight. Then, the solvent was removed under reduced pressure and an aqueous solution of 1 M HCl was added. The white precipitate was filtered and dried under vacuum to obtain the carboxylic acid **21** (4.26 g, 90%). Its spectroscopic data were in concordance with those described in bibliography.[7]

Compound 22

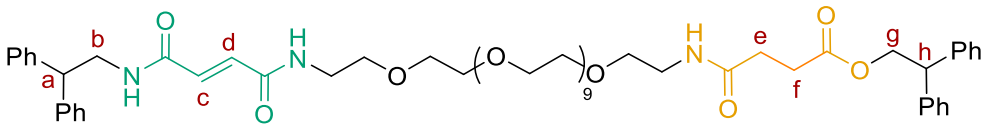

22

To a suspension of carboxylic acid **21** (127 mg, 0.43 mmol) in dry DCM (10 mL) under N_2 atmosphere, the amine **10** (320 mg, 0.39 mmol) and DMAP (80 mg, 0.67 mmol) were added, and the solution was stirred at 0 ºC for 5 min. Afterwards, EDCI·HCl (130 mg, 0.67 mmol) was added at 0 ºC and the reaction was stirred at room temperature for 24 hours. The mixture was washed with 1 M HCl (2 x 100 mL), $NaHCO_3$ (sat. aq.) (2 x 100 mL) and brine (1 x 100 mL). The organic phase was dried over anhydrous $MgSO_4$ and concentrated under reduced pressure. The crude was purified by column chromatography on silica gel using a $CHCl_3$/MeOH 92/8 mixture as eluent, to furnish the compound **22** as colourless oil (172 mg, 40%).

^{1}H NMR (400 MHz, DMSO-d_6, 298 K) δ = 8.48 (m, 2H, NH), 7.90 (t, J = 5.6 Hz, 1H, NH), 7.39 – 7.22 (m, 16H, H_{Ar}), 7.25 – 7.08 (m, 4H, H_{Ar}), 6.75 (d, J = 5.6 Hz, 1H, H_c or H_d), 6.74 (d, J = 5.6 Hz, 1H, H_c or H_d), 4.57 (d, J = 7.6 Hz, 2H, H_g), 4.32 (t, J = 7.6 Hz, 1H, H_h), 4.21 (t, J = 7.9 Hz, 1H, H_a), 3.80 (dd, J = 7.9, 5.6 Hz, 2H, H_b), 3.49 (s, 44H, EG-H), 3.27 (m, 2H, EG-H), 3.16 (m, 2H, EG-H), 2.37 (t, J = 6.8 Hz, 2H, H_f), 2.27 (t, J = 6.8 Hz, 2H, H_e).

^{13}C NMR (100 MHz, DMSO-d_6, 298 K) δ = 172.3 (C=O), 170.6 (C=O), 163.8 (C=O), 142.8 (C), 141.6 (C), 132.6 (CH), 128.5 (CH), 128.0 (CH), 127.9 (CH), 126.6 (CH), 126.4 (CH), 69.8 (CH_2), 69.7 (CH_2), 69.6 (CH_2), 69.1 (CH), 68.9 (CH_2), 66.1 (CH_2), 50.0 (CH), 49.3 (CH), 43.4 (CH_2), 29.7 (CH_2), 29.0 (CH_2).

HRMS (ESI) calculated for $C_{60}H_{83}N_3O_{16}Na$ $[M+Na]^+$ 1124.5666, found 1124.5633.

Compound 23

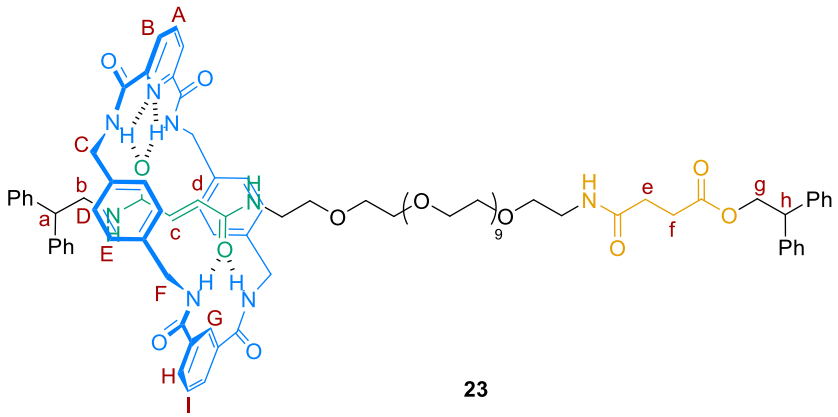

23

Thread **22** (27 mg, 0.025 mmol) and Et_3N (0.2 mL, 1.44 mmol) were dissolved in $CHCl_3$ (6 mL, stabilized with amylenes). The mixture was stirred vigorously whilst solutions of (25 mg, 0.13 mmol) in $CHCl_3$ (3 mL) and diamine **14** (50 mg, 0.13 mmol) in $CHCl_3$ (3 mL) were simultaneously added over a period of 4 hours using motor-driven syringe pumps. After 12 hours, the solvent was removed under reduced pressure and the resulting residue was purified by column chromatography on silica gel using a DCM/MeOH 92/8 mixture as eluent, to furnish the rotaxane **23** as colourless oil (12 mg, 29%).

^{1}H NMR (400 MHz, 3/2 (v/v) D_2O/DMSO-d_6, 298 K) δ = 9.66 (bs, 1H, NH), 8.28 (m, 3H, H_{A+B}), 8.19 (m, 4H, NH), 8.34 7.99 (m, 2H, NH), 7.18 (m, 24H, $H_{G+H+I+Ar}$), 6.88 (m, 8H, H_{D+E}), 5.90 (m, 2H, H_{c+d}), 3.63 (m, 2H, PEG-H), 3.46–4.29 (m, 38H, PEG-H), 3.14 (m, 8H, PEG-H), 2.23 (t, *J* = 7.1 Hz, 2H, H_f), 2.13 (t, *J* = 7.1 Hz, 2H, H_e). ***Signals corresponding to protons a, b, g, and h could not be assigned due to overlap with the residual solvent peaks.***

Although the conditions employed in optical tweezers experiments cannot be fully replicated in bulk measurements, both in terms of [molecular shuttle]/[BHMF] ratio and solvent polarity, the reactivity of BHMF for [4+2] cycloadditions under aqueous conditions was evaluated using the following procedure (**Figure S5.2**): 12 mg of molecular shuttle **23** were dissolved in 0.6 mL of a mixture 3/2 (v/v) D_2O/DMSO-d_6 in an NMR tube and ^{1}H NMR spectrum was registered (**Figure S5.3a**). Next, 55 mg (60 equiv.) of BHMF were added to the tube and the mixture was heated and stirred at 45 ºC for 2 hours and another ^{1}H NMR spectrum was registered (**Figure S5.3b**), in which the disappearance of the fumaramide double bond protons signals (in green) was observed.

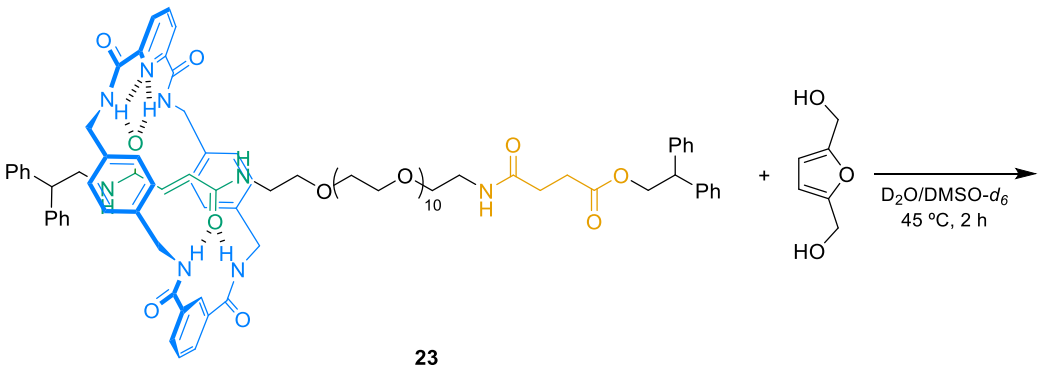

23

Figure S5.2. Reaction of molecular shuttle model **23** with BHMF in aqueous medium.

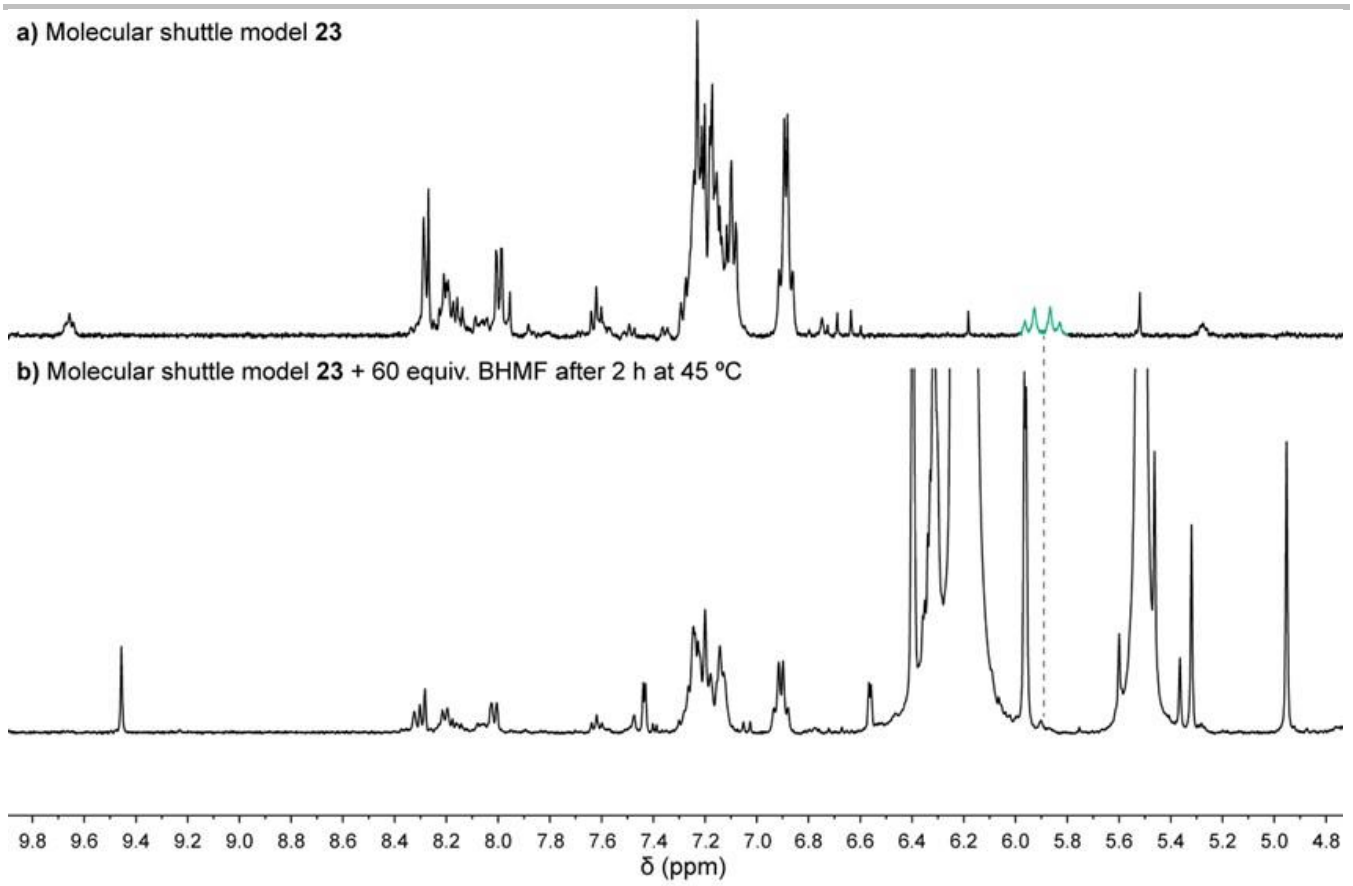

Figure S5.3. Partial ^{1}H NMR spectra (400 MHz, 3/2 (v/v) D_2O/DMSO-d_6, 298 K) of **a)** molecular shuttle model **23**; **b)** molecular shuttle model **23** incubated with 60 equiv. of BHMF at 45 ºC for 2 hours. The fumaramide signals highlighted in green at 5.90 ppm disappeared after [4+2] cycloaddition with BHMF under such conditions.

S6. Pulling-relaxing cycles of individual molecular shuttles and fitting to the WLC model

Individual molecular shuttle-dsDNA hybrid attachments should show a response in force-extension curves (pulling-relaxing cycles) that fit a worm-like chain model (WLC, **eq. 1**) describing the elastic properties of the DNA handles:

$$x = L_c \cdot \left[1 - \frac{1}{2} \cdot \sqrt{\frac{K_B T}{F \cdot L_p}} + \frac{F}{S}\right] \quad \textbf{(eq. 1)}$$

where x and F are the extension and force; $L_c = 0.34 \cdot bp$ is the contour length (being bp the number of base pairs), L_p the persistence length and S the stretching modulus, and $K_B T = 4.114\, pN \cdot nm = 0.14\, kcal/mol$.[8]

The mechanical strength of the H-bonding interaction between macrocycle and stations as well as the coexistence force were determined from the histogram in **Figure S6.1**, constructed with all the breaking forces gathered from the pulling-relaxing cycles (59 total curves) of 7 individual molecular shuttle-dsDNA hybrids.

The gaussians peaks fitted to the breaking force histograms yield the rupture forces at each station (F_{succ} in orange and F_{fum} in green). The coexistence force ($F_{1/2}$) is calculated as the intersection point of both gaussian distributions (grey dashed line).

To assess whether repeated pulling–relaxing cycles collected from the same molecule introduced bias through intra-sample autocorrelation, we additionally analyzed the rupture data on a per-molecule basis. The mean breaking forces for both the *fum* and *succ* stations, as well as the coexistence force, were calculated for each of the 7 independent molecules separately. The overall mean and standard deviation were then calculated across these 7 per-molecule averages (**Table S6.1**). This per-molecule analysis yields values in very good agreement with the pooled Gaussian analysis of all 59 cycles reported in the main text and in **Figure S6.1**. This confirms that intra-sample autocorrelation does not materially bias the reported breaking forces or their uncertainties.

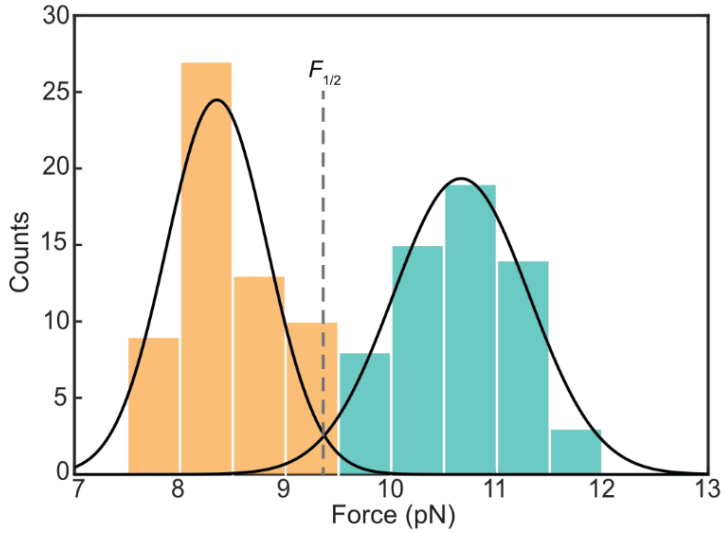

Figure S6.1. Determination of breaking forces at each station. Orange (*succ*) and green (*fum*) histograms represent the breaking rupture forces obtained for each station in pulling-relaxing cycles of 7 individual molecules at a loading rate of 200 nm s^{-1} (*N* = 59). Each histogram fits to a gaussian distribution yielding: $F_{succ} = 8.3 \pm 0.7$ pN and $F_{fum} = 10.7 \pm 0.8$ pN. The intersection point between the two gaussian fits (grey dashed line) reveals the coexistence force, $F_{1/2} = 9.4 \pm 0.8$ pN.

Parameter	Gaussian Distribution	Per-molecule Analysis
F_{fum}	10.7 ± 0.8 pN	10.7 ± 0.3 pN
F_{succ}	8.3 ± 0.7 pN	8.4 ± 0.3 pN
$F_{1/2}$	9.4 ± 0.8 pN	9.6 ± 0.3 pN

Table S6.1. Comparison and determination of breaking forces at each station and the coexistence force, based on a Gaussian distribution of the 59 values obtained for 7 different molecules, along with the per-molecule statistical analysis.

Figure S6.2 displays individual pulling-relaxing cycles taken in aqueous conditions at 20 mM Tris-HCl 150 mM NaCl before and after Diels–Alder adduct formation by movement of the optical trap at a constant velocity of 200 nm s^{-1} at 22 ± 1 ºC. Black curves correspond to the pulling cycle and blue curves correspond to the relaxing cycle. Green and orange lines are the fit to the WLC before and after shuttling, respectively, before reaction. Orange lines are the fit to the WLC after reaction.

At low pulling forces the force-extension curves were fitted to a WLC model. To accurately extract shuttling distances, the persistence length (L_p) and stretch modulus (S) of the DNA handles were not treated as free fitting parameters, but were fixed at $L_p = 50\,nm$ and $S = 1100\,pN$, which are characteristic and established values for a single dsDNA molecule under these buffer conditions (green curves, equation 1).[9] After the shuttling, the experimental data have been adjusted to a modified model considering a WLC response (eq. 1 for the DNA handles) plus a constant Δx accounting for the displacement of the curve due to the shuttling of the macrocycle between stations in the molecular shuttle.

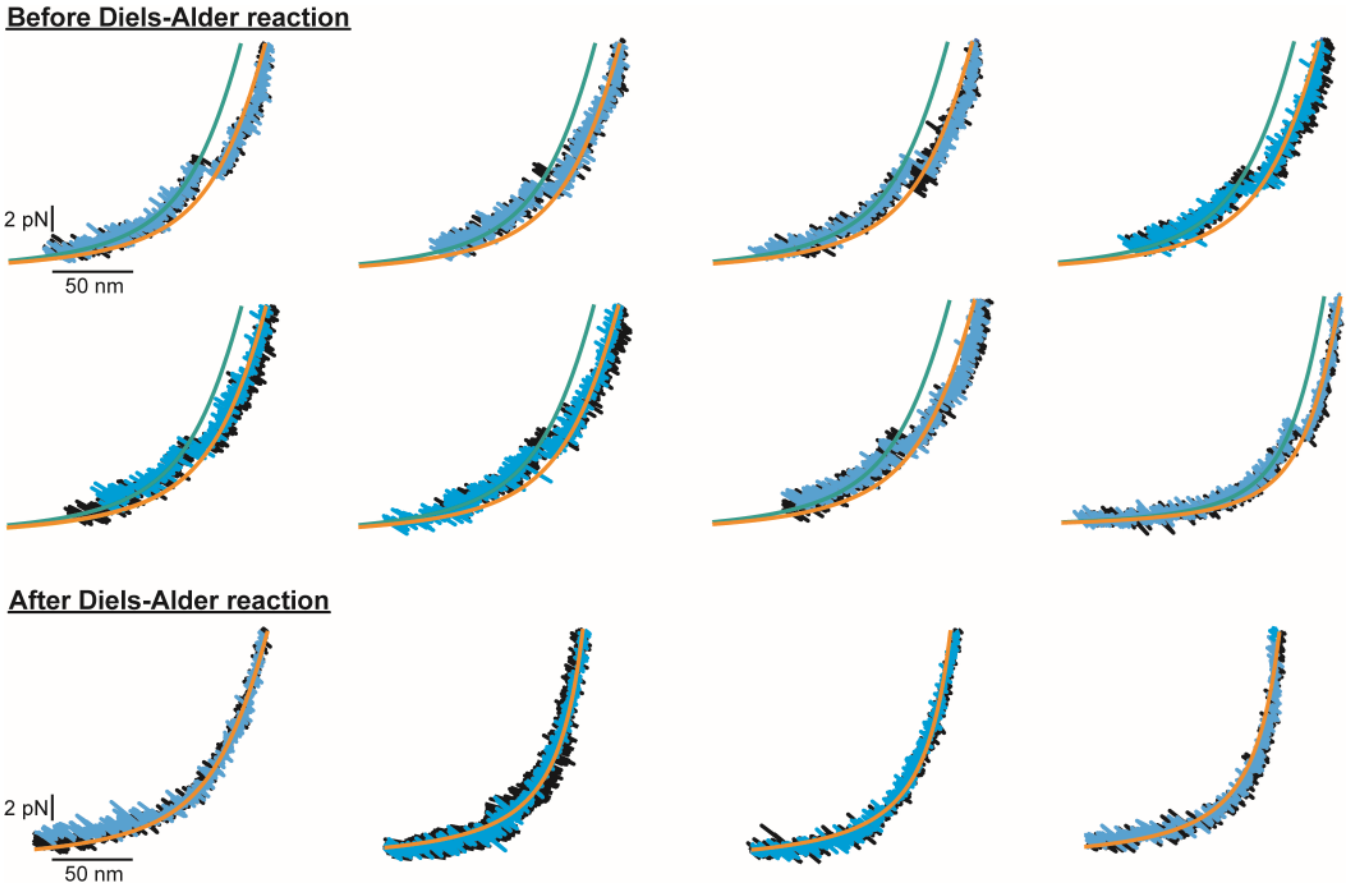

Figure S6.2. Examples of pulling-relaxing cycles of individual molecular shuttles. Pulling curves are represented in black and relaxing curves are in blue. Fitting to the WLC model is displayed by green and orange lines for pulling and relaxing curves, respectively.

S7. Dependence of DNA handles length in apparent shuttling distance

Analysis of the pulling-relaxing curves (Figure 2 in main text) using a WLC model provided an apparent shuttling distance of 15 ± 0.1 nm. Moreover, the experimental shuttling distance recovered from hopping traces (Figure 3 in main text) is 15.2 ± 0.8 nm, in both cases far from the theoretical maximum distance of 5.5 nm, calculated by DFT (**Section S12 and Figure S2.2**). We attribute this increase of the shuttling distance to the extended and soft dsDNA handles required for manipulating the molecular shuttle. Notably, when shorter (and stiffer) dsDNA handles are used, the expected distance is successfully recovered. **Figure S7.1** displays hopping traces of the molecular shuttle-dsDNA hybrid using both 3538 bp (2701 upper + 837 lower) handles and 120 bp (60 bp upper + 60 bp lower) handles. The distances recovered between stations are 15.2 ± 0.8 nm, and 5.3 ± 0.8 nm for long and short handles, respectively. Therefore, the length of the DNA handles used affects the measured extension, and shorter (and stiffer) handles allow us to recover the theoretical values expected for distance between stations. The length of pulling handles is known to affect the measured length in single-molecule force spectroscopy, through changes in stiffness and persistence length that affects the mechanical construct bead-handle-molecule.[10-13] A comprehensive empirical model accounting for this effect is currently on development in our laboratory, but it is beyond the scope of this work. Importantly, although longer handles introduce this artifact, they greatly facilitate detection and manipulation and do not hinder the observation of shuttling or the occurrence of the Diels–Alder reaction. For these reasons, we continued to employ such long dsDNA handles.

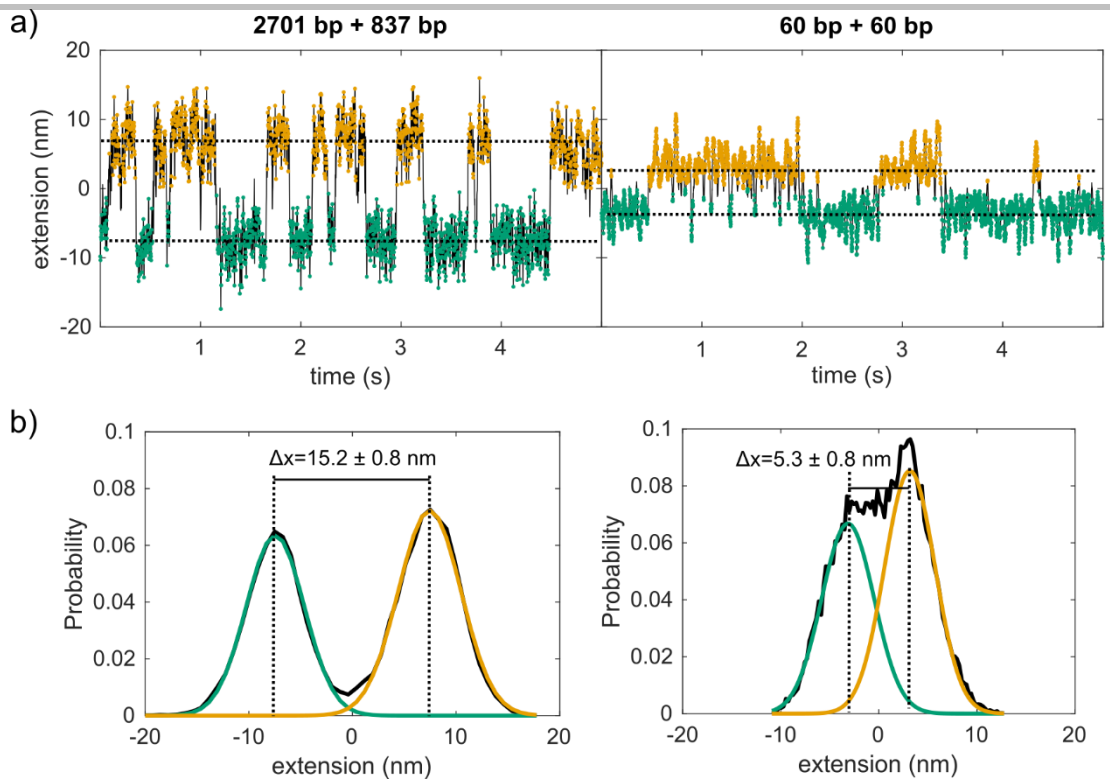

Figure S7.1. a) Extension *vs* time traces of a molecular shuttle-dsDNA hybrid using a total number of base pairs in both handles of 3538 (left, 2701 bp top handle and 837 bp bottom handle) and 120 (right, 60 bp top handle and 60 bp bottom handle). Dashed lines indicate the center of the gaussian probability distributions at the *fum* (green) and *succ* (orange) stations. **b)** Normalized probability distributions of the traces in **a)**. Black line corresponds to the experimental data and green and orange lines to gaussian fits for *fum* and *succ*, respectively. The distance between the gaussian distributions is 15.2 ± 0.8 and 5.3 ± 0.8 nm for long and short handles, respectively.

S8. Calculation of the thermodynamic parameters from constant force experiments

Constant force measurements (hopping traces) allow the extraction of the shuttling kinetics as well as the main parameters governing the energy landscape of the system. This mode also allows the gathering of hundreds of events of individual association/dissociation processes in real time. The population distribution at each station is well described by gaussian probability distributions (**Figure 3 d-f** in main text) where the shuttling dynamics of the macrocycle is inferred by measuring the change in molecular extension. To obtain the shuttling rates for *fum* and *succ* stations, we first calculate the residence times at each station. This is done by monitoring every single shuttling event within a trace and measuring the residence time at each station in between events (**Figure S8.1. a-c** shows 5 seconds segments of the traces in **Figure 3** main text, green and orange dots represent data points at the *fum* and *succ* stations, respectively). The histogram of the residence times fits well to an exponential decay, whose decay constant equals the shuttling rates at each station (k_{succ} and k_{fum}) which is the inverse of the residence time at each station (**Figure S8.1. d-f**, dots represent measured residence times and solid lines the fitting to exponential functions).[14] The values for k for each station and trace are summarized in **Table S8.1**.

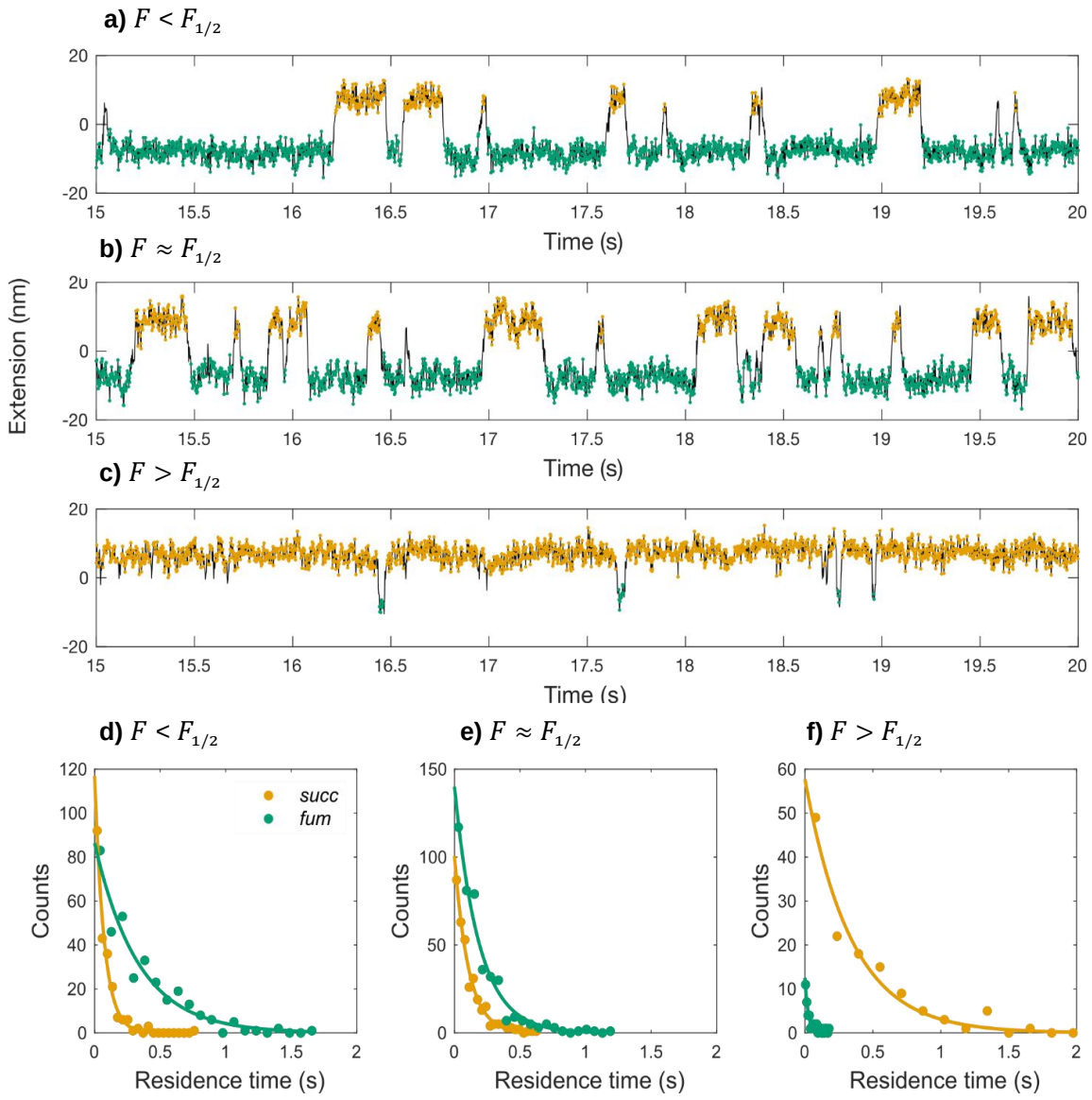

Figure S8.1. Segments of 5 seconds of the hopping traces at **a)** $F < F_{1/2}$; **b)** $F \approx F_{1/2}$; and **c)** $F > F_{1/2}$, depicted in the main text (**Figure 3**). Green and orange dots represent the data points at the *fum* and *succ* stations that are considered for the calculation of the residence times. Residence time distributions obtained for the *fum* (green) and *succ* (orange) stations at constant force: **d)** $F < F_{1/2}$; **e)** $F \approx F_{1/2}$; and **f)** $F > F_{1/2}$. Solid lines represent fitting to the exponential decay.

		$F < F_{1/2}$	$F \approx F_{1/2}$	$F > F_{1/2}$
k (s^{-1})	k_{succ}	13.9 ± 1.7	9 ± 1	2.9 ± 0.5
	k_{fum}	3.0 ± 0.6	5.3 ± 0.7	41 ± 10

Table S8.1. Summary of shuttling rates at 3 different force regimes.

As expected from Bell-Evans theory,[14-17] the kinetic rates depend exponentially on the applied force ($\ln k \propto F$; **Figure S8.2**). The intersection between k_{succ} and k_{fum} fitting functions yields the coexistence force and corresponding kinetic rate ($F_{1/2} = 9.41 \pm 0.02\, pN$ and $k_{1/2} = 7.7 \pm 0.8\, s^{-1}$). Despite the reduced number of experimental data points, the value of coexistence force recovered from this method (starting from the hopping traces in **Figure 3** of the main text) matches perfectly with the value recovered from pulling-relaxing experiments ($F_{1/2} = 9.4 \pm 0.8\, pN$, **section S6**), hence validating the recovered kinetic rates values.

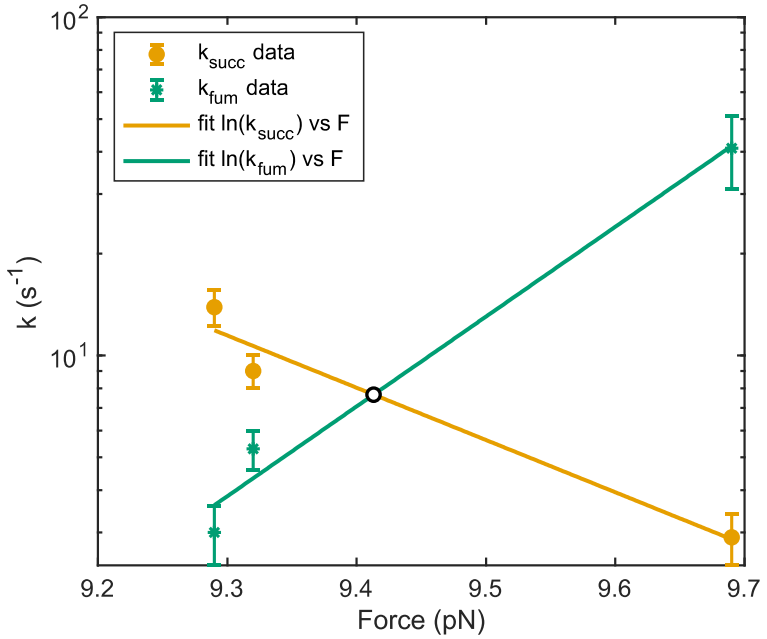

Figure S8.2. Experimentally deduced kinetic rates detailed in **Table S8.1** (green and orange dots for k_{fum} and k_{succ}, respectively) as a function of applied force. The data fits well with exponential functions (solid lines, note logarithmic *y*-scale). The crossing point yields the coexistence force and the corresponding kinetic rate.

S9. Study of the transition-path times

The transition-path time of the shuttling between stations (τ) is defined as the time it takes for the macrocycle to travel from one thermodynamic state to another.[18] From the hopping traces in **Figure 3** in main text, we can directly measure transit times as the time required to cross between a and b boundaries. These boundaries defining the transition-path are chosen as half the mean position of *fum* and *succ* stations (indicated by dashed horizontal lines in **Figure S9.1**, left panels). A complete description on the transit time calculation and analysis can be found in our previous work.[19] **Figure S9.1** (right panels) contain the histograms of transit times across the hopping traces in **Figure 3** (main text) acquired at 3 different force regimes. In all cases, the transit times present broad distributions, indicating that each transition across the barrier is statistically independent and highly variable. They also show symmetry for the 3 force values (i.e. *fum* → *succ* distribution is the same as *succ* → *fum* distribution) in accordance with the principle of microscopic reversibility. The last transition before Diels–Alder reaction

takes a time that is comparable with the broad distribution of transit times (vertical black dashed line in right panels in **Figure S9.1**), indicating that the Diels–Alder reaction does not, at least within experimental resolution, affect the transit of the macrocycle between stations.

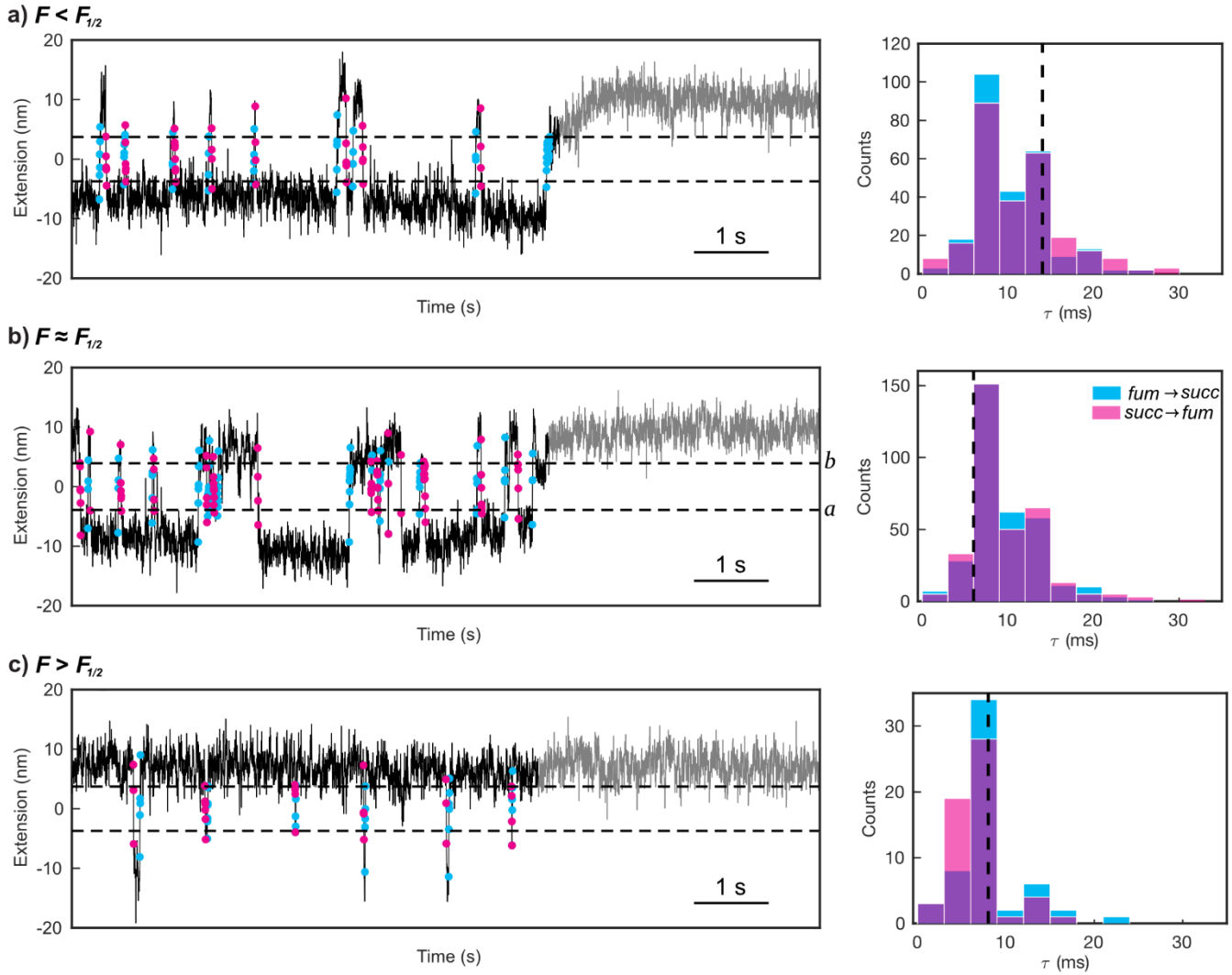

Figure S9.1. Representative hopping traces (10 s segments extracted from the traces shown in **Figure 3** of the main text; left panels) and the corresponding histograms of transition-path times (right panels) at: **a)** $F < F_{1/2}$; **b)** $F \approx F_{1/2}$; and **c)** $F > F_{1/2}$. Pink dots denote *succ* → *fum*, whereas blue dots denote *fum* → *succ* transitions. The transition-paths boundaries a and b defining transition-paths are chosen as half of the mean extension of *fum* and *succ* stations, as indicated by dashed horizontal lines in the left panels. Vertical dashed lines in the right panels mark the time of the final transition preceding the Diels–Alder reaction (formation of *add*). Overlapping regions are highlighted in purple.

Estimation of instrumental bandwidth limits:

In single-molecule force spectroscopy, the measurement of rapid molecular transition-path times (TPTs) can be convoluted by the physical relaxation of the microspheres and the viscoelasticity of the long dsDNA handles.[18, 20-21] To ensure our measurements were not limited by instrumental filtering, we estimated the passive relaxation time of the system. At the high forces used in our constant-force experiments (>9 pN), the dsDNA handles are highly extended, restricting their longitudinal viscoelastic

relaxation to the microsecond regime. The physical response is therefore dominated by the hydrodynamic drag of the microsphere.[18, 22] For a 3 μm polystyrene bead in aqueous buffer held at a trap stiffness of k = 0.135 pN/nm, the characteristic hydrodynamic relaxation time is approximately 0.2 ms. This value is obtained considering $\tau = \gamma/\kappa$ with the drag coefficient $\gamma = 6\pi\eta R$, using $\eta = 8.9 \cdot 10^{-4}$ Ns/m^2 as viscosity of the aqueous buffer and R=1.5 μm as bead radius.[23] This physical limit (0.2 ms) is an order of magnitude faster than our 8-10 ms mean TPTs. Furthermore, at our data acquisition rate of 500 Hz (2 ms temporal resolution), the measured TPT distributions span from 2 to 30 ms, and we clearly resolve individual rapid shuttling events occurring in ~2 ms. If the 8-10 ms mean TPT were an artificial limit imposed by the viscoelastic drag of the handles and beads, all transits would be smeared to slower limits, precluding the observation of 2 ms events. Because the system can physically resolve these rapid transits, the final TPT measured immediately prior to the reaction can be directly compared to the pre-reaction distribution without requiring theoretical deconvolution.

S10. NMR spectra

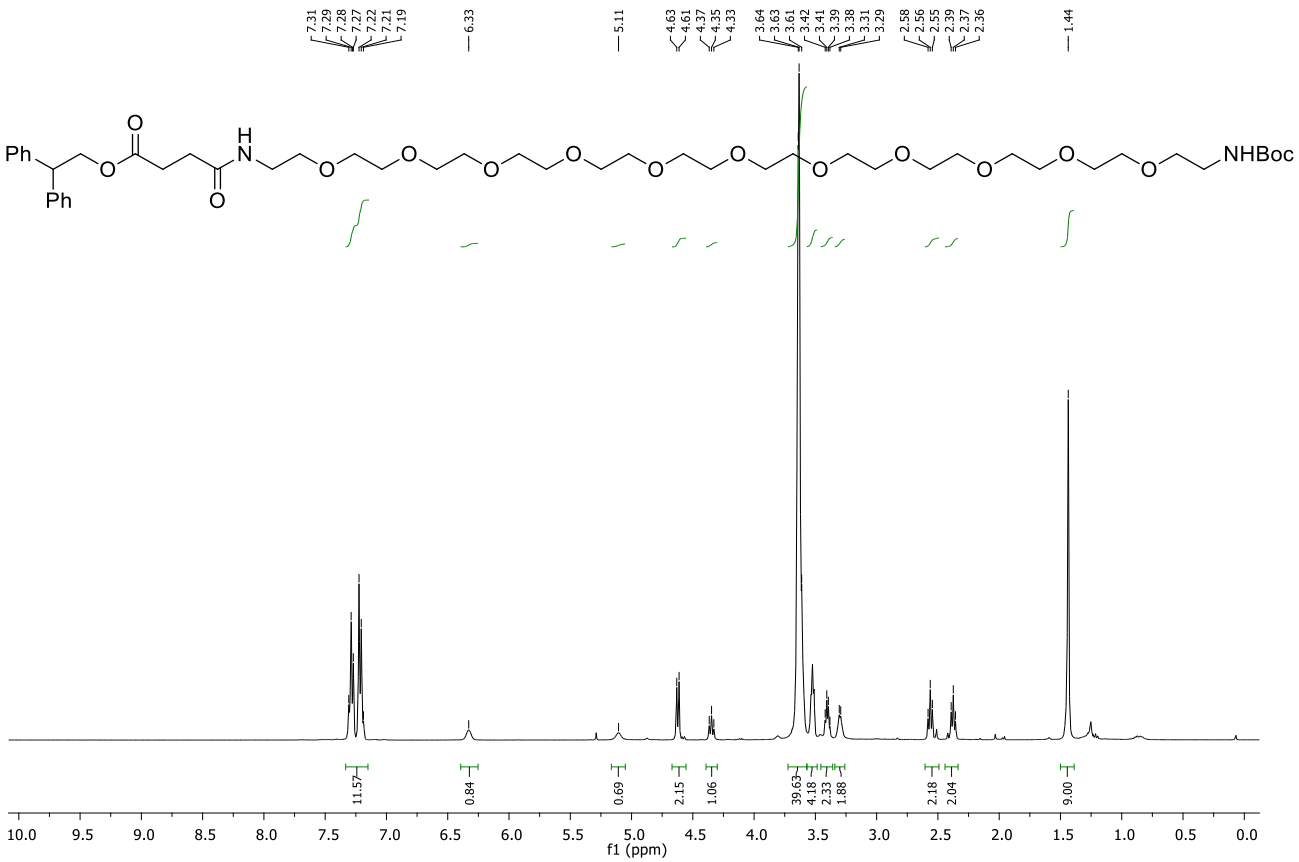

Figure S10.1. ^{1}H NMR spectrum of the compound **9** (400 MHz, $CDCl_3$, 298 K).

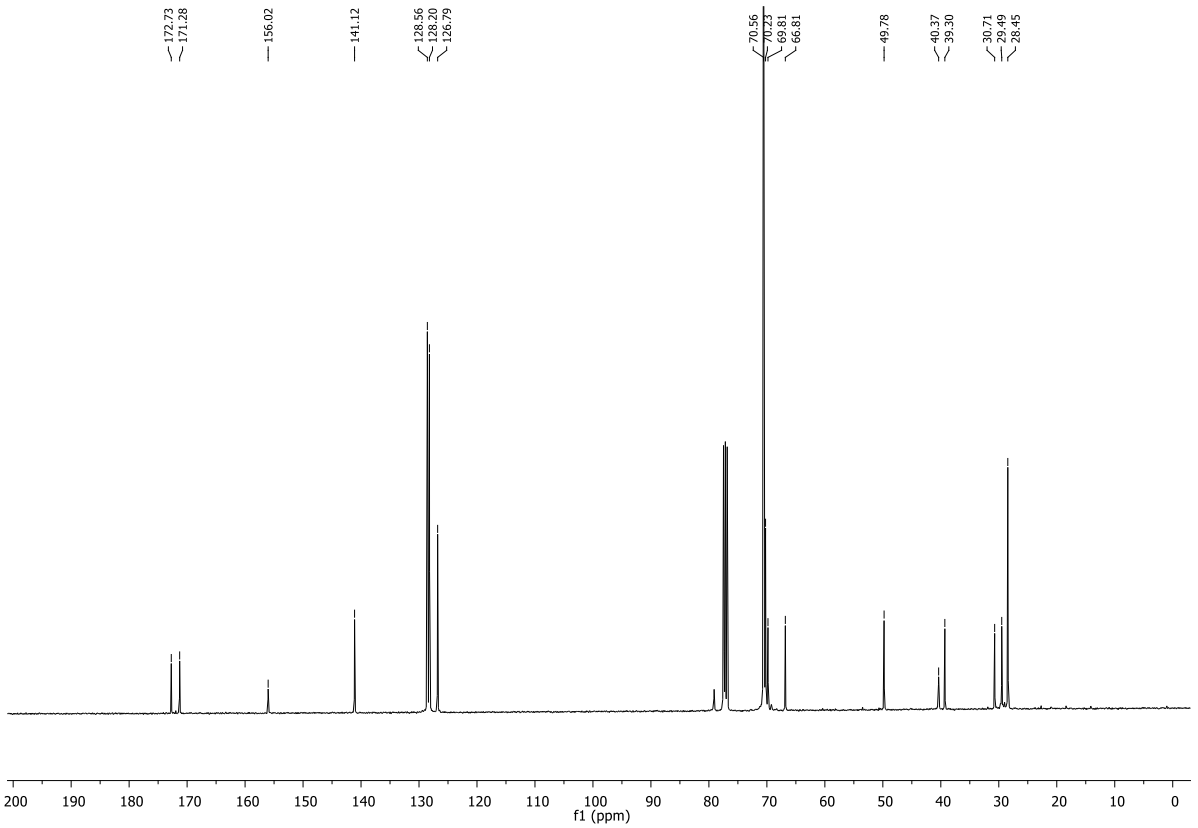

Figure S10.2. ^{13}C NMR spectrum of compound **9** (100 MHz, $CDCl_3$, 298 K).

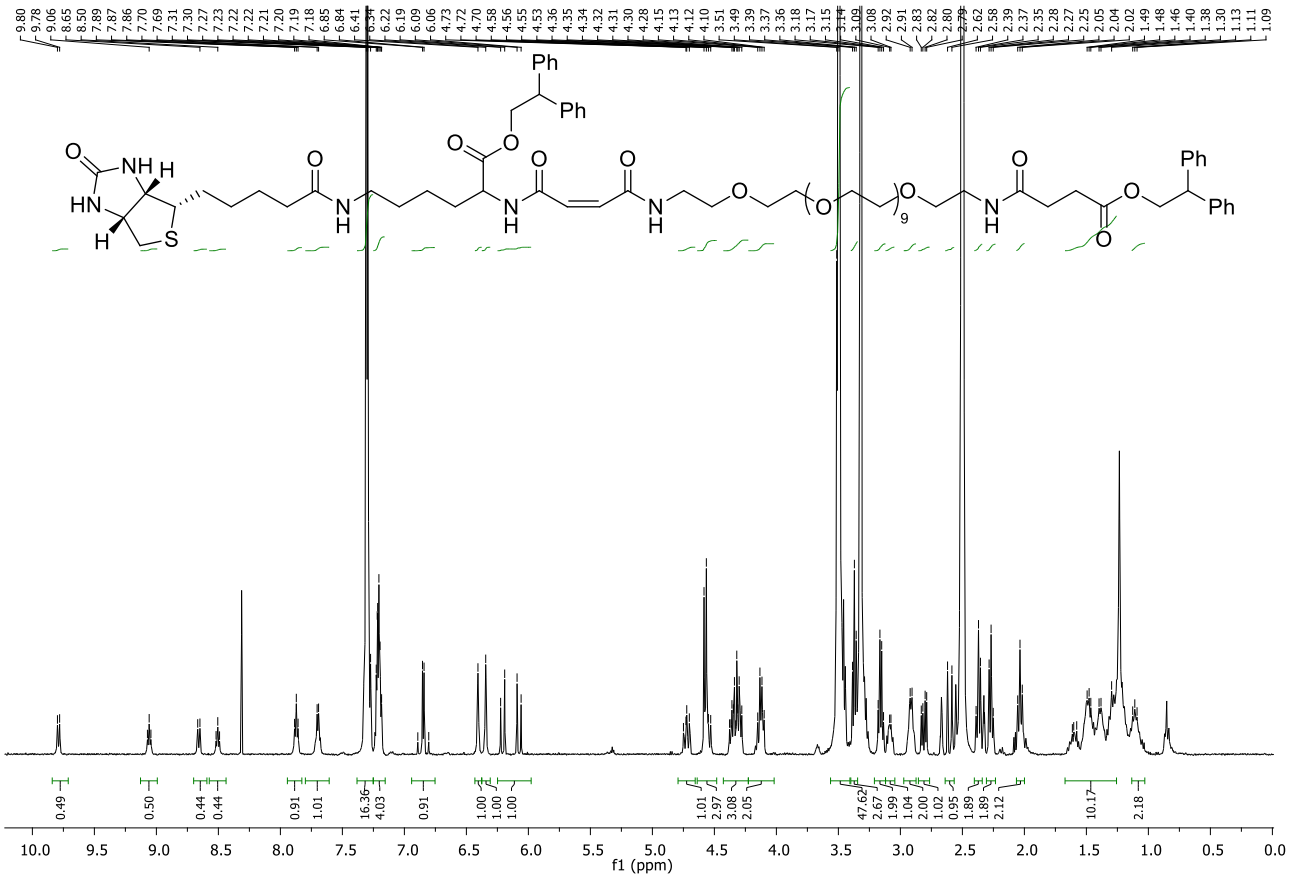

Figure S10.3. ^{1}H NMR spectrum of compound **11** (400 MHz, DMSO-d_6, 298 K).

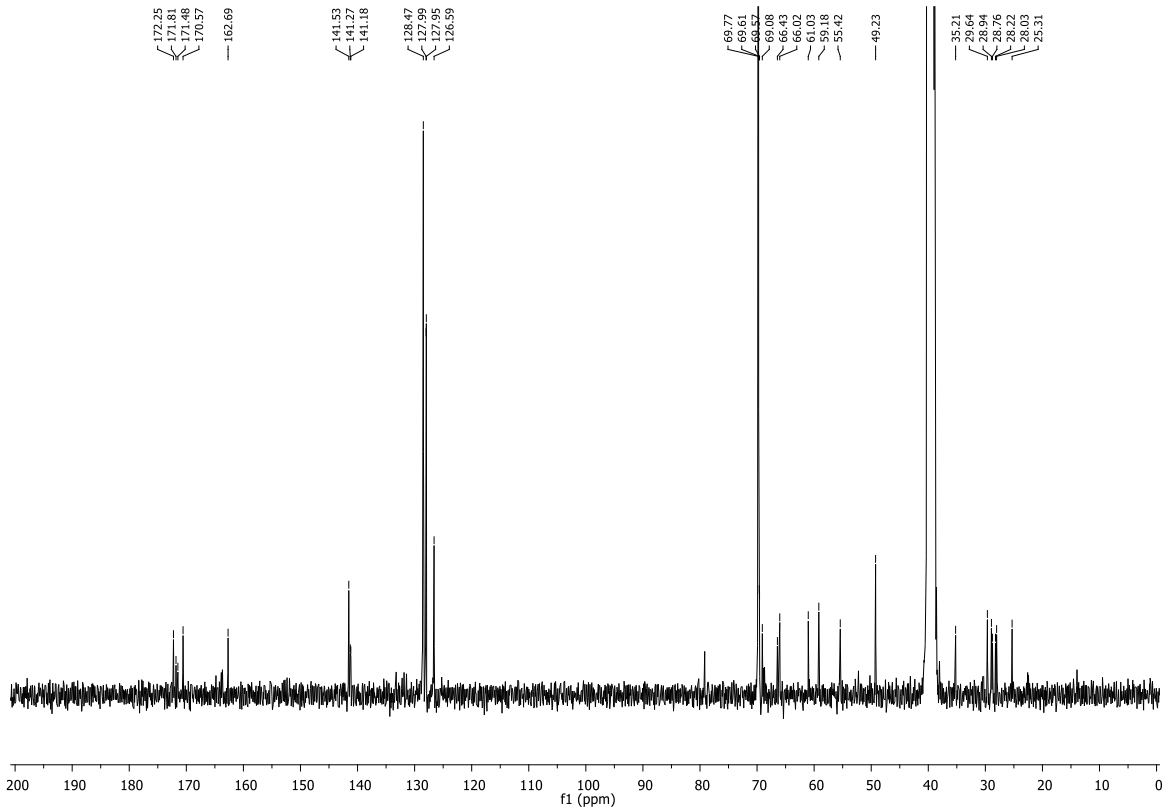

Figure S10.4. ^{13}C NMR spectrum of compound **11** (100 MHz, DMSO-d_6, 298 K).

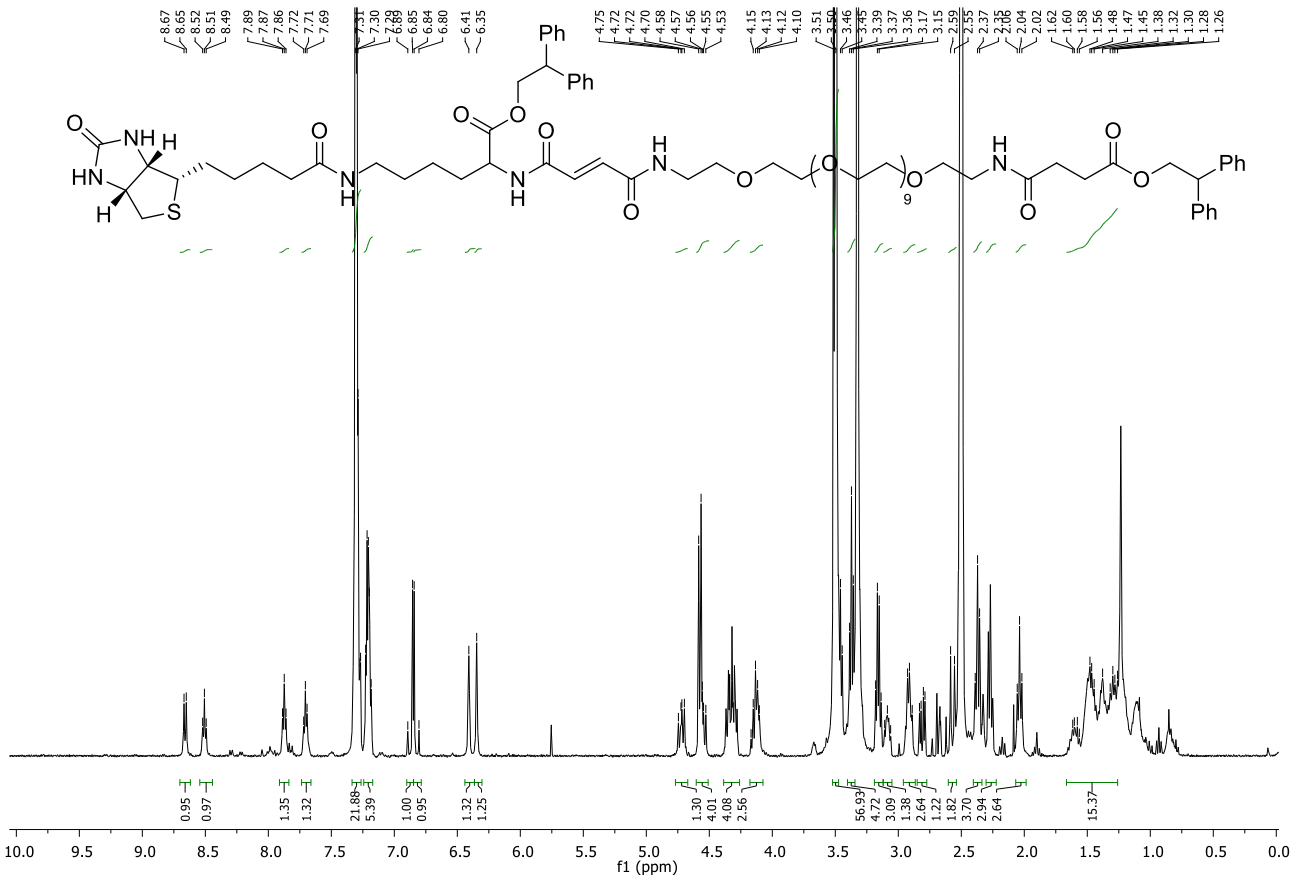

Figure S10.5. ^{1}H NMR spectrum of compound **12** (400 MHz, DMSO-d_6, 298 K).

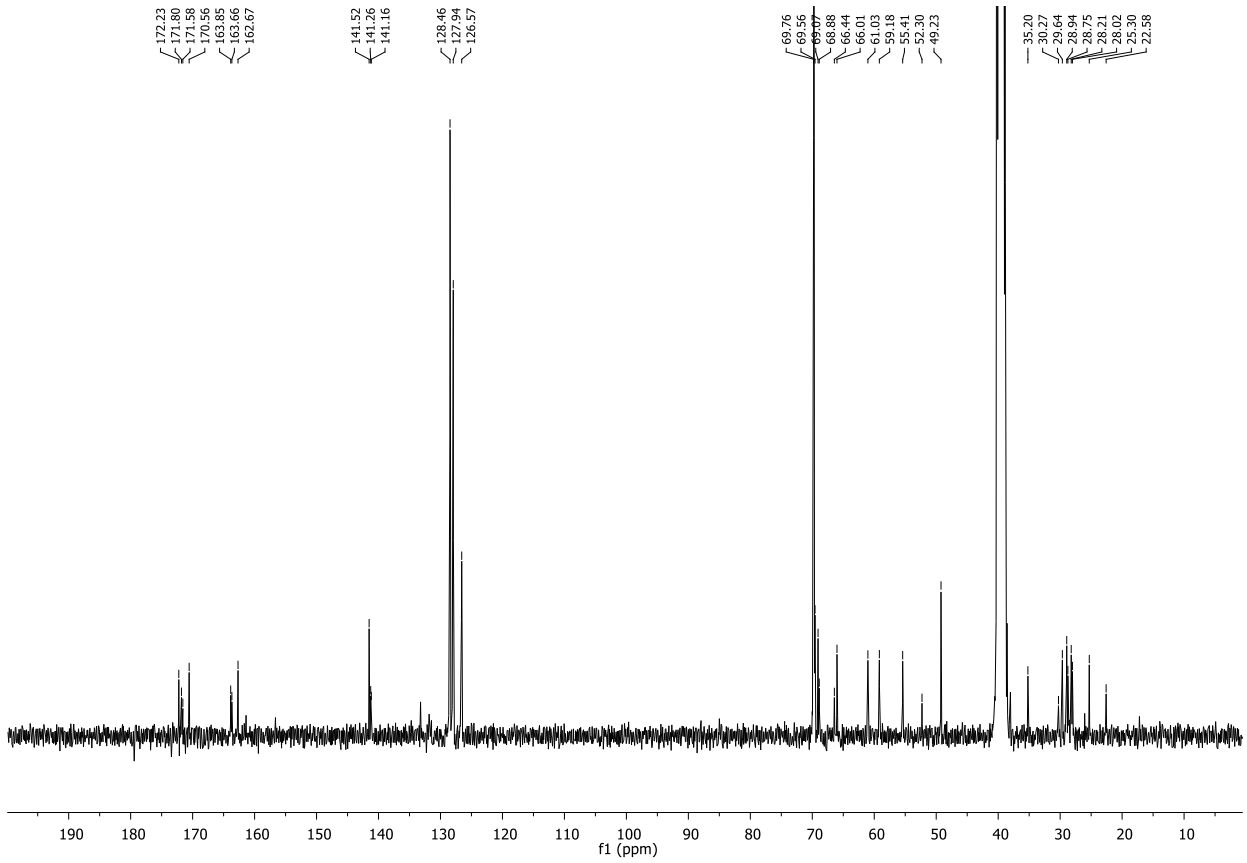

Figure S10.6. ^{13}C NMR spectrum of compound **12** (100 MHz, DMSO-d_6, 298 K).

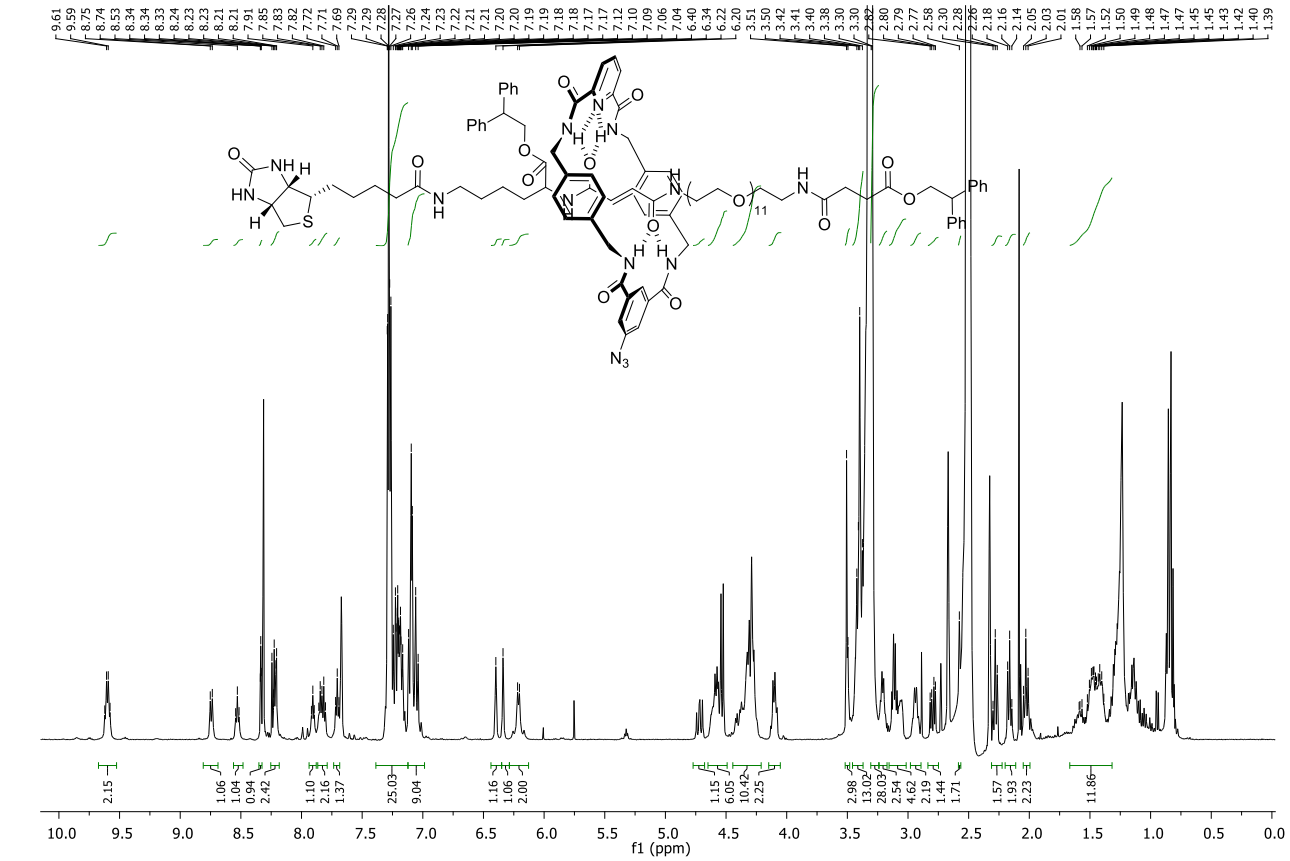

Figure S10.7. ^{1}H NMR spectrum of compound **15** (400 MHz, DMSO-d_6, 298 K).

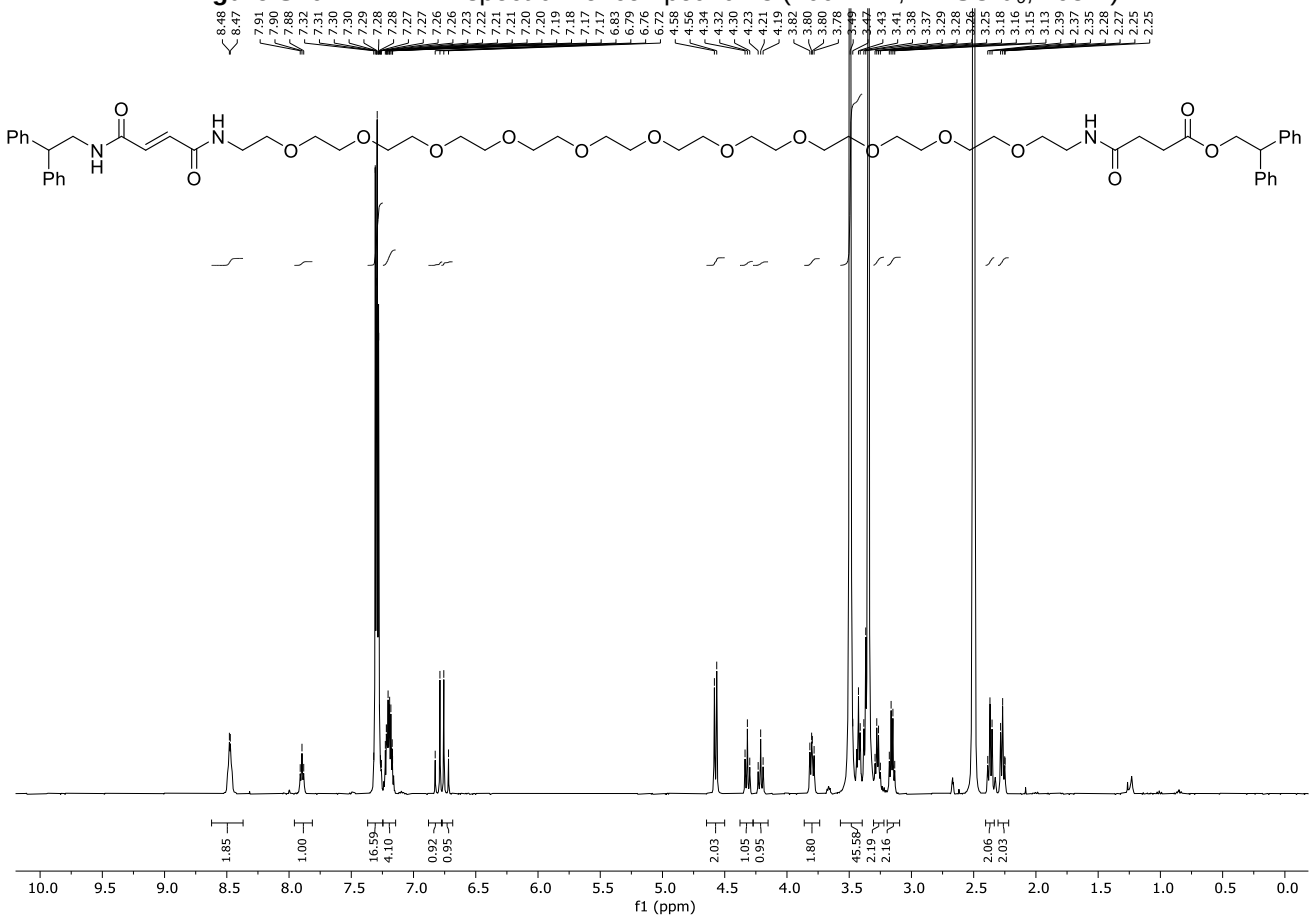

Figure S10.8. ^{1}H NMR spectrum of the compound **22** (400 MHz, DMSO-d_6, 298 K).

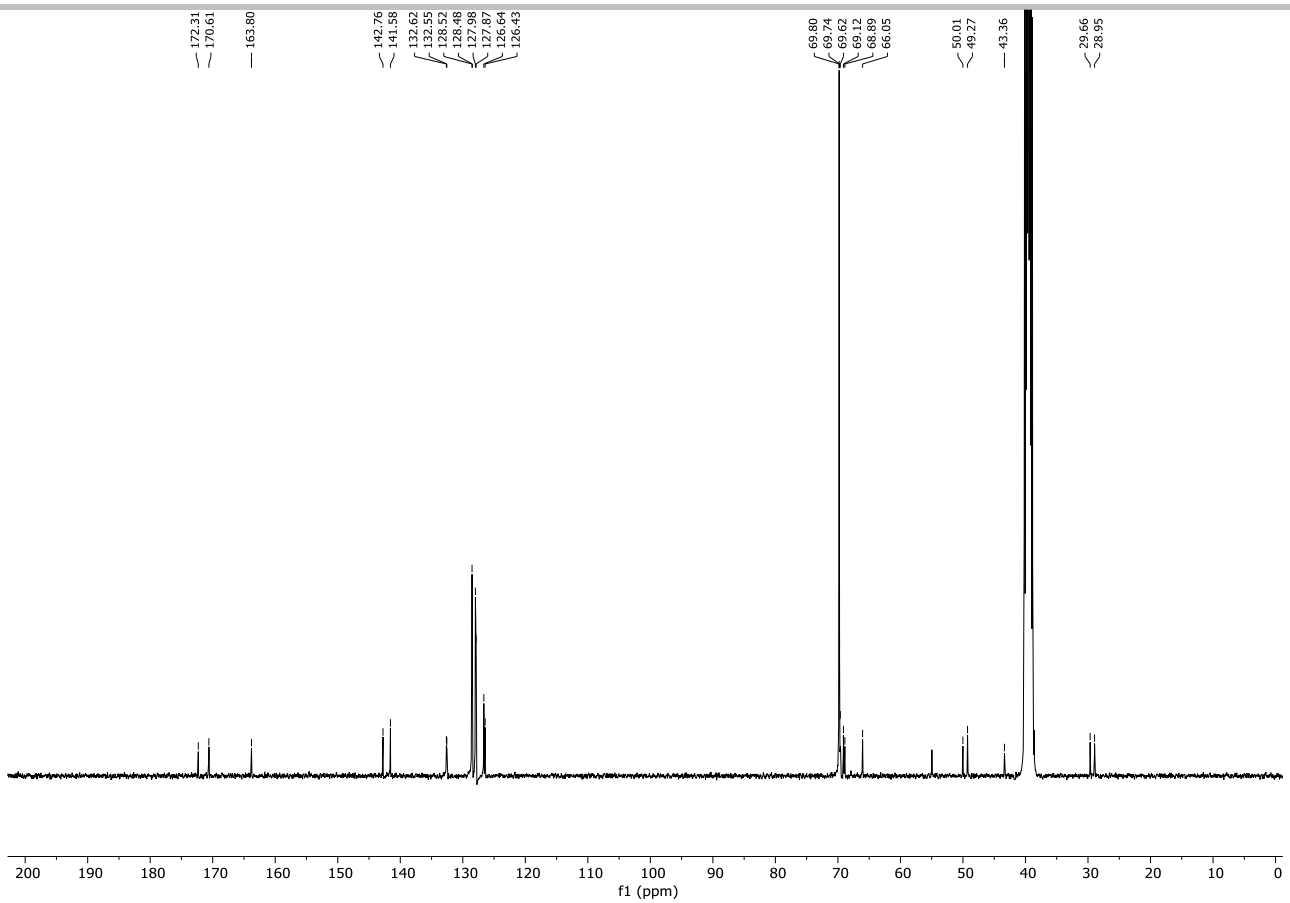

Figure S10.9. ^{13}C NMR spectrum of compound **22** (100 MHz, DMSO-d_6, 298 K).

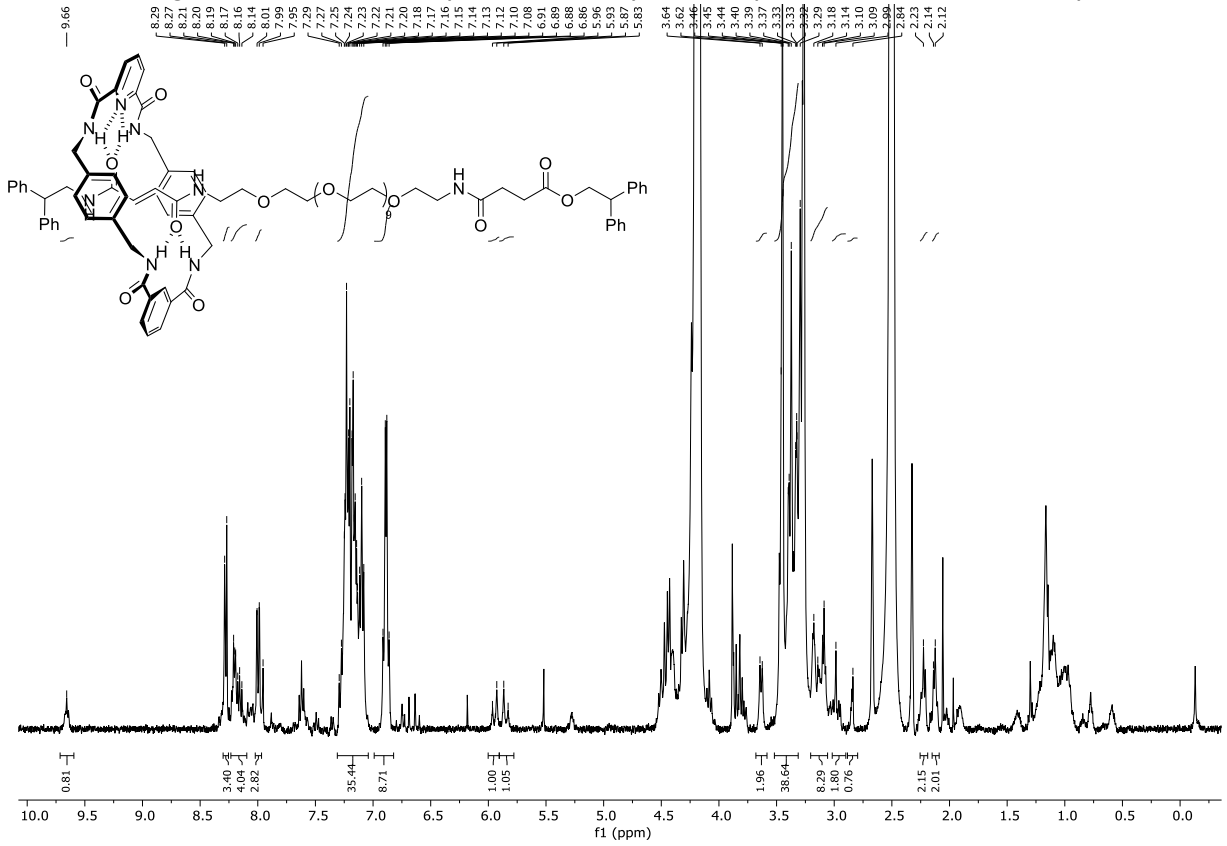

Figure S10.10. ^{1}H NMR spectrum of compound **23** (400 MHz, 3/2 (v/v) D_2O/DMSO-d_6, 298 K).

S11. High Resolution Mass Spectrometry

Unless otherwise stated, the spectrum at the top corresponds to the experimental isotopic distribution and the one at the bottom corresponds to the theoretical isotopic distribution.

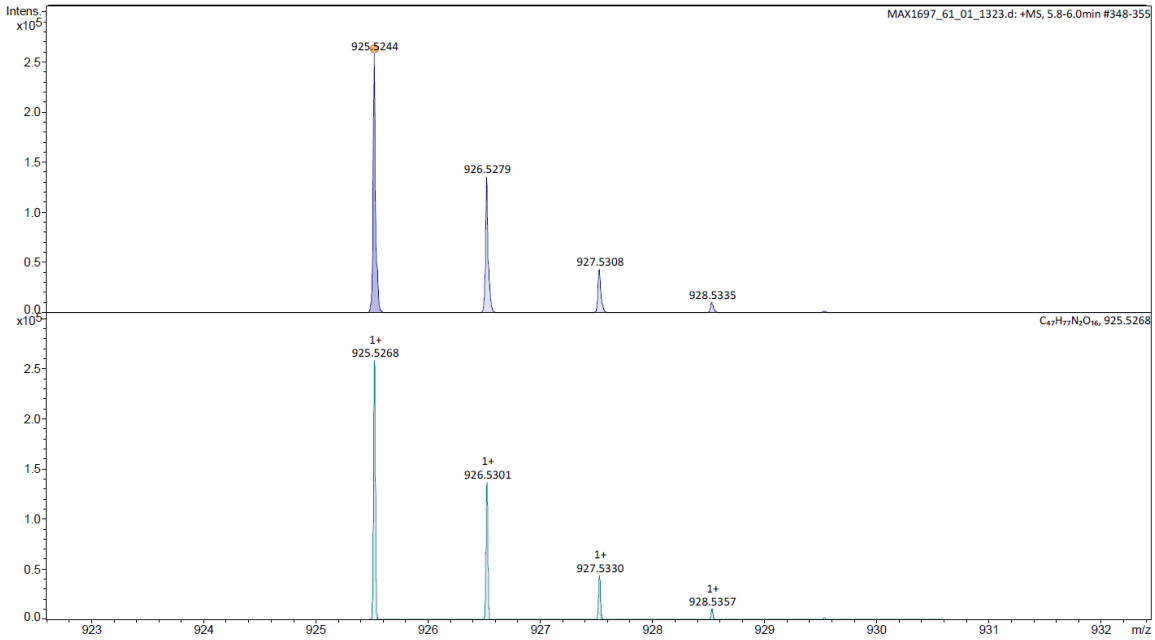

Figure S11.1. HRMS (APCI) spectra of compound **9**.

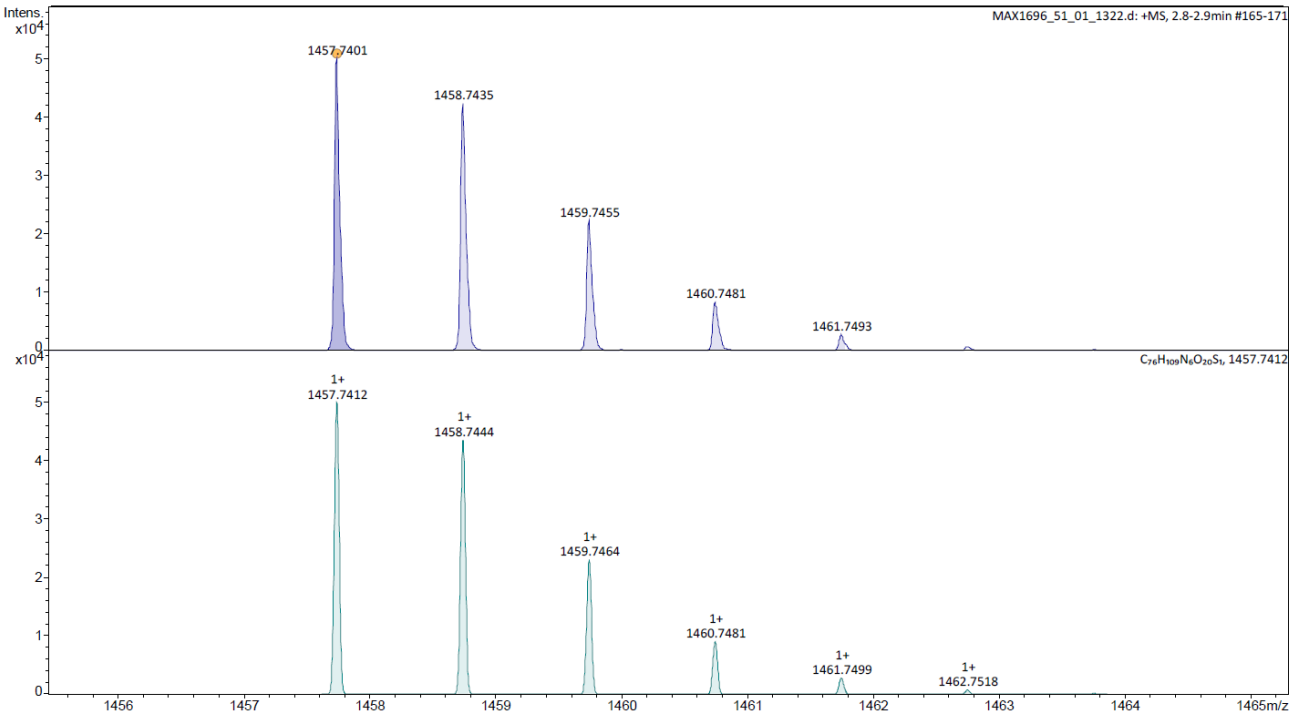

Figure S11.2. HRMS (APCI) spectra of compound **11**.

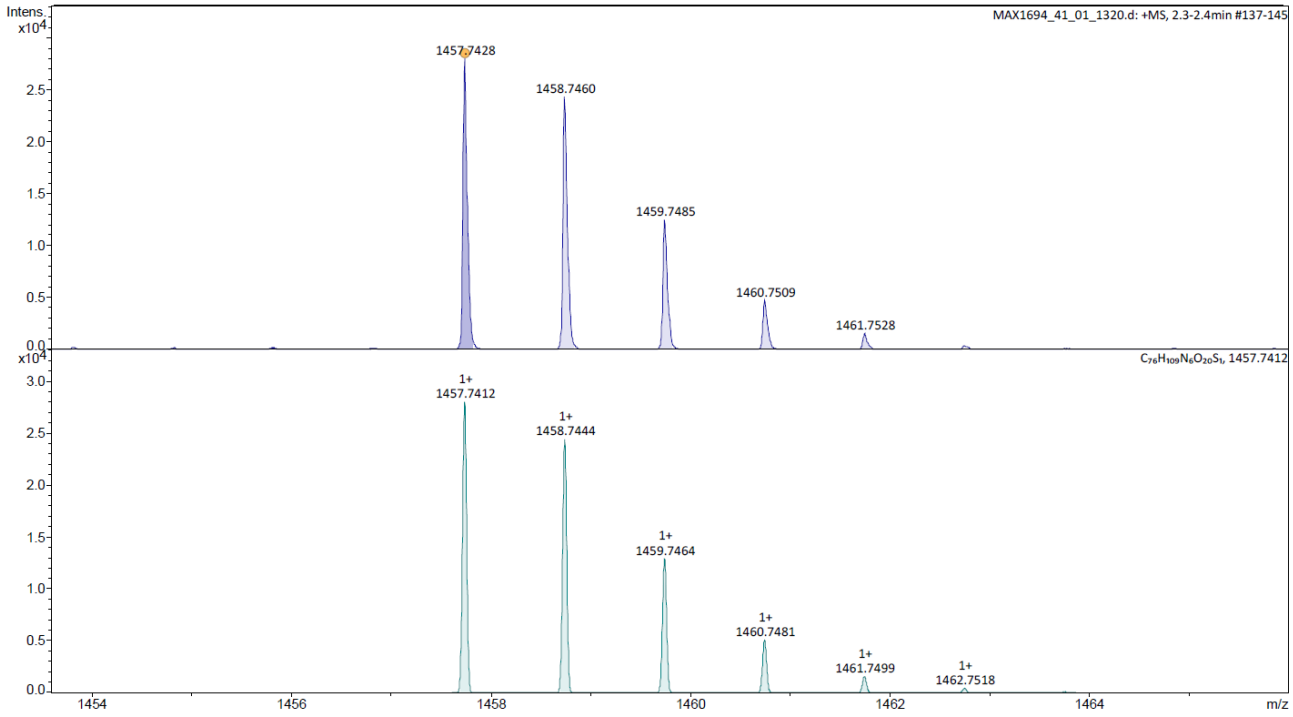

Figure S11.3. HRMS (APCI) spectra of compound **12**.

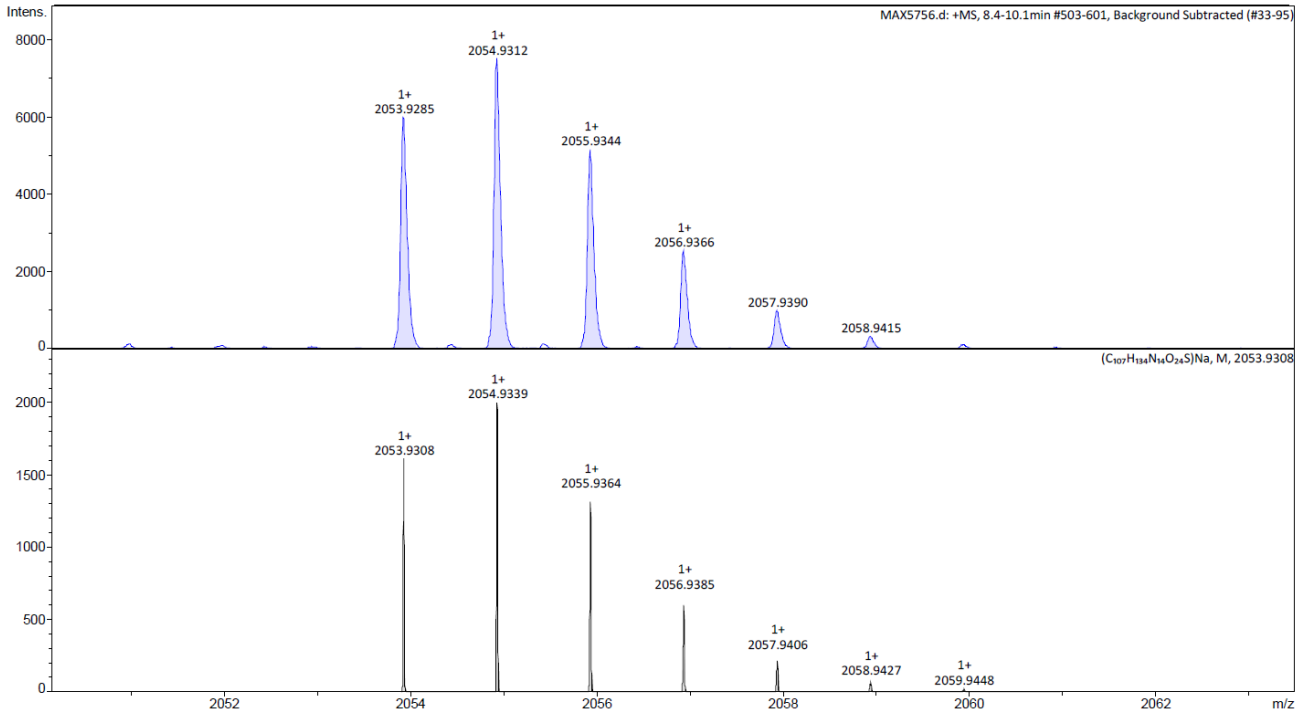

Figure S11.4. HRMS (ESI) spectra of compound **15**.

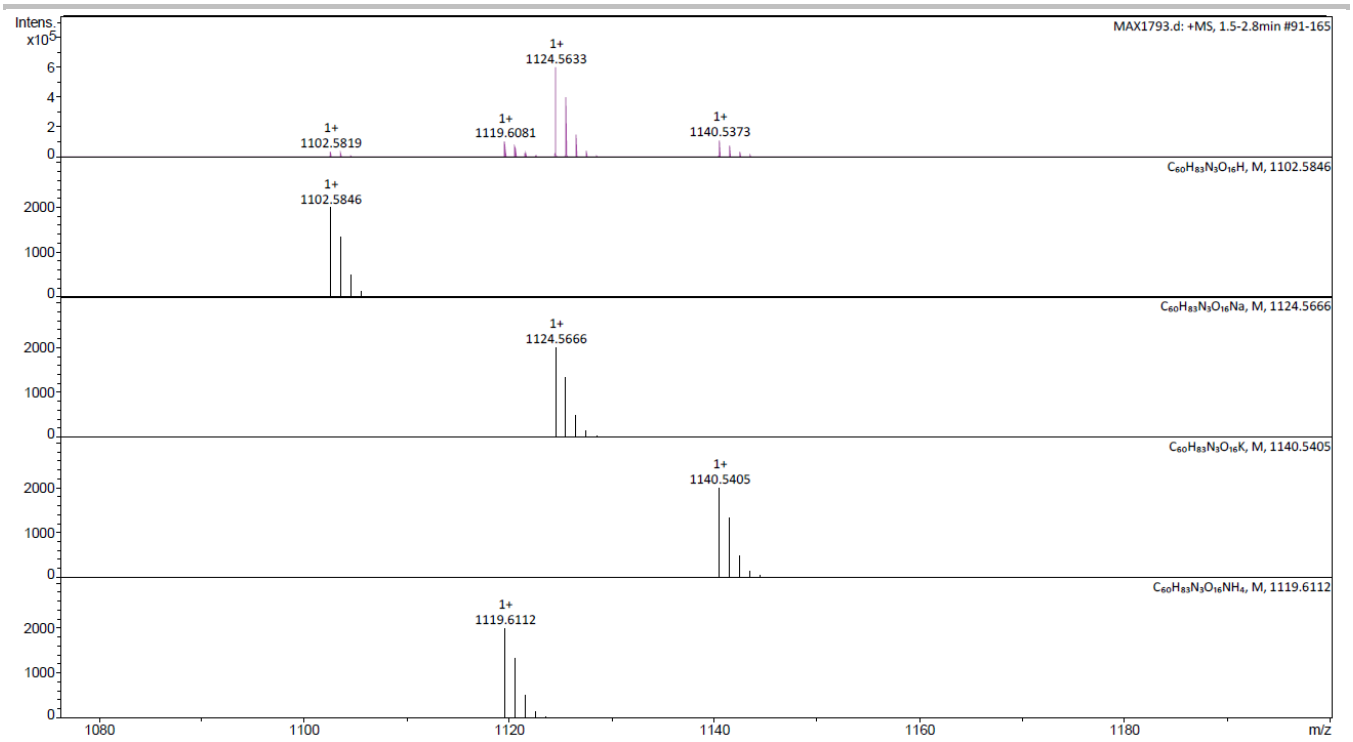

Figure S11.5. HRMS (ESI) spectra of compound **22**.

S12. Cartesian coordinates of thread 12

The Gaussian 09 program[24] was used for geometry optimization. Energy minimization was performed at the density functional theory (DFT) B3LYP/6-31G(d,p) level of theory. The DFT optimized geometries were found to have zero imaginary frequencies.

Atom	x	y	z
N	20.61565	-3.5953	-0.11357
C	19.75479	-2.53602	0.3968
C	19.91776	-1.20583	-0.35179
C	18.99263	-0.11077	0.1925
C	19.17338	1.22477	-0.5356
C	18.25437	2.34808	0.00419
N	18.55131	2.69852	1.38598
C	17.78012	2.60237	2.51837
C	21.89687	-3.76299	0.3318
C	22.67928	-4.90057	-0.32273
C	24.13248	-4.50085	-0.60547
C	24.993	-5.66693	-1.10425
C	26.44288	-5.2414	-1.38855
C	27.36324	-6.38924	-1.84891
C	27.37705	-6.69562	-3.37723
C	28.38171	-5.72358	-4.09209
C	29.31055	-5.07463	-3.04471
S	29.15426	-6.0739	-1.50602
N	26.16009	-6.45099	-4.12312

C	26.20024	-5.30874	-4.90058
N	27.48564	-4.78408	-4.75758
O	25.29601	-4.84658	-5.57185
H	27.71492	-7.72863	-3.50333
H	28.97983	-6.28829	-4.81933
O	22.38014	-3.06981	1.22126
C	18.37251	3.56339	-0.92039
O	17.66846	3.73985	-1.88968
O	19.39909	4.35749	-0.54969
C	19.70147	5.52005	-1.35955
C	21.17889	5.49154	-1.77788
O	18.15975	3.10655	3.57306
C	16.4969	1.84336	2.43134
C	15.70853	1.73917	3.50551
C	14.4325	0.96813	3.44071
N	13.72487	0.94882	4.61205
O	14.04944	0.38965	2.42627
C	12.45619	0.25066	4.73359
C	11.26886	1.11922	4.31389
O	10.09524	0.35955	4.52767
C	8.9128	1.02956	4.13259
C	7.74579	0.09015	4.39605
O	6.56178	0.76669	4.01958
C	5.39325	-0.00929	4.2032
C	4.208	0.83818	3.76653
O	3.04004	0.06043	3.94663
C	1.8547	0.73912	3.57837
C	0.69151	-0.21232	3.81383
O	-0.49494	0.46807	3.45218
C	-1.66051	-0.31635	3.61762
C	-2.84902	0.53625	3.2002
O	-4.01361	-0.25101	3.35939
C	-5.20153	0.43078	3.0054
C	-6.36059	-0.53153	3.21571
O	-7.54937	0.15093	2.86588
C	-8.71143	-0.64294	3.0098
C	-9.90282	0.2121	2.60579
O	-11.06368	-0.58473	2.74286
C	-12.25364	0.09736	2.39627
C	-13.40821	-0.87566	2.58037
O	-14.5988	-0.19344	2.23635
C	-15.75691	-0.99704	2.35637
C	-16.95048	-0.1422	1.95845
O	-18.10732	-0.94846	2.07219
C	-19.29851	-0.26841	1.72574
C	-20.44811	-1.25225	1.8812
O	-21.63999	-0.57172	1.53825
C	-22.79331	-1.38598	1.62905

C	-23.98751	-0.53449	1.22579
O	-25.14145	-1.34806	1.32204
C	-26.33218	-0.68016	0.95222
C	-27.47083	-1.69767	1.03269
N	-28.76716	-1.1108	0.73093
C	-29.22989	-0.99162	-0.54996
C	-30.57165	-0.27564	-0.68993
C	-31.31881	-0.72904	-1.94123
C	-32.40833	0.2372	-2.35025
O	-33.23487	-0.33828	-3.25222
C	-34.31485	0.4532	-3.79396
C	-35.64006	-0.31063	-3.65594
C	-36.06095	-0.60807	-2.21906
O	-28.60267	-1.41278	-1.51609
O	-32.52183	1.37657	-1.94508
C	-36.71338	0.43946	-4.44865
C	-36.90287	-1.70539	-1.9847
C	-37.35391	-2.0082	-0.70197
C	-36.96781	-1.21467	0.38052
C	-36.12779	-0.12405	0.1632
C	-35.67672	0.17821	-1.12492
C	-37.01293	0.04967	-5.76039
C	-37.9526	0.74822	-6.51959
C	-38.60753	1.8534	-5.97566
C	-38.31709	2.25144	-4.66953
C	-37.37873	1.55005	-3.91253
C	21.57462	4.28802	-2.6289
C	22.89335	3.81712	-2.54911
C	23.32558	2.74636	-3.32914
C	22.44084	2.11981	-4.2092
C	21.12569	2.57389	-4.29554
C	20.69438	3.64846	-3.51262
C	21.51891	6.83439	-2.43053
C	22.08274	7.85876	-1.65886
C	22.35842	9.10779	-2.21634
C	22.07034	9.35189	-3.5594
C	21.50828	8.33884	-4.33799
C	21.23553	7.09046	-3.7785
H	20.30642	-4.12663	-0.91319
H	18.71621	-2.88226	0.34288
H	20.0089	-2.39929	1.4512
H	20.96392	-0.89042	-0.26453
H	19.72069	-1.3622	-1.42117
H	17.94633	-0.43643	0.10326
H	19.18422	0.0305	1.26315
H	20.21503	1.55981	-0.458
H	18.96282	1.10219	-1.60483
H	17.21559	2.02729	-0.07443

H	19.39262	3.24339	1.53185
H	22.66172	-5.74539	0.37933
H	22.18551	-5.24508	-1.2403
H	24.14674	-3.69289	-1.34856
H	24.55386	-4.08169	0.31422
H	24.9941	-6.46787	-0.35072
H	24.53583	-6.09336	-2.00555
H	26.45394	-4.43468	-2.1306
H	26.86217	-4.81994	-0.46883
H	27.11409	-7.30024	-1.29363
H	29.00155	-4.04308	-2.85926
H	30.35835	-5.07777	-3.35179
H	25.27909	-6.90621	-3.95077
H	27.81419	-4.21091	-5.52144
H	19.02057	5.55069	-2.21076
H	19.51548	6.39519	-0.73167
H	21.75938	5.43165	-0.84923
H	16.18097	1.35016	1.51834
H	16.01443	2.22114	4.43131
H	14.06957	1.47814	5.39862
H	12.49343	-0.63479	4.09542
H	12.32368	-0.07444	5.76964
H	11.24699	2.04996	4.90633
H	11.37575	1.3977	3.25477
H	8.77392	1.96199	4.70265
H	8.94377	1.2943	3.06434
H	7.87703	-0.83664	3.8158
H	7.7248	-0.18573	5.46231
H	5.43013	-0.93276	3.6041
H	5.27148	-0.30253	5.25794
H	4.16913	1.76032	4.36767
H	4.33119	1.13386	2.71272
H	1.71526	1.65192	4.17888
H	1.88028	1.03948	2.519
H	0.82852	-1.12287	3.20945
H	0.66925	-0.5167	4.87217
H	-1.62006	-1.22563	2.99732
H	-1.78127	-0.63441	4.66522
H	-2.89289	1.44324	3.82361
H	-2.72575	0.85817	2.15409
H	-5.34626	1.32828	3.62731
H	-5.17558	0.7565	1.95355
H	-6.21711	-1.42738	2.59118
H	-6.38447	-0.86008	4.26677
H	-8.66367	-1.53846	2.3703
H	-8.83462	-0.98405	4.04983
H	-9.9543	1.1052	3.24836
H	-9.77689	0.55713	1.56739

H	-12.40692	0.9812	3.03545
H	-12.22386	0.44452	1.3514
H	-13.25542	-1.75816	1.93927
H	-13.43671	-1.225	3.62459
H	-15.69836	-1.88029	1.70092
H	-15.88613	-1.35801	3.38894
H	-17.01249	0.73898	2.61641
H	-16.81872	0.22208	0.92739
H	-19.46412	0.60307	2.37871
H	-19.26086	0.09715	0.68746
H	-20.28339	-2.12182	1.22564
H	-20.48403	-1.62076	2.91863
H	-22.71834	-2.25882	0.9617
H	-22.93493	-1.76303	2.65435
H	-24.0604	0.34104	1.89057
H	-23.84841	-0.16177	0.19914
H	-26.52962	0.17093	1.62668
H	-26.26518	-0.28683	-0.07331
H	-27.28577	-2.49818	0.31343
H	-27.50061	-2.13518	2.03497
H	-29.30301	-0.7013	1.48109
H	-31.18544	-0.41519	0.2071
H	-30.37892	0.80128	-0.76527
H	-30.60375	-0.81553	-2.76807
H	-31.75616	-1.72473	-1.82072
H	-34.33687	1.42653	-3.30211
H	-34.0959	0.60744	-4.85444
H	-35.49032	-1.27725	-4.15231
H	-37.21057	-2.32618	-2.82268
H	-38.00452	-2.8642	-0.54683
H	-37.31588	-1.44802	1.38252
H	-35.81506	0.49755	0.99755
H	-35.00574	1.02032	-1.25982
H	-36.50693	-0.8117	-6.19028
H	-38.17456	0.42607	-7.53297
H	-39.34167	2.39748	-6.56259
H	-38.82552	3.10787	-4.23595
H	-37.17309	1.85698	-2.89141
H	23.58948	4.30056	-1.868
H	24.35145	2.39895	-3.24728
H	22.7731	1.28317	-4.81659
H	20.42576	2.09119	-4.97166
H	19.65873	3.96462	-3.58438
H	22.31175	7.67498	-0.61166
H	22.80121	9.88672	-1.6023
H	22.28622	10.32193	-3.99732
H	21.28524	8.51809	-5.38582
H	20.8156	6.30408	-4.39822

S13. References

[1] T. Naranjo, K. M. Lemishko, S. de Lorenzo, A. Somoza, F. Ritort, E. M. Perez, B. Ibarra, *Nat. Commun.* **2018**, *9*, 4512.

[2] J. A. Morin, F. J. Cao, J. M. Lazaro, J. R. Arias-Gonzalez, J. M. Valpuesta, J. L. Carrascosa, M. Salas, B. Ibarra, *Proc. Natl. Acad. Sci. U. S. A.* **2012**, *109*, 8115-8120.

[3] S. B. Smith, Y. Cui, C. Bustamante, in *Methods in Enzymology, Vol. 361*, Academic Press, **2003**, pp. 134-162.

[4] H. Mao, J. Ricardo Arias-Gonzalez, S. B. Smith, I. Tinoco, C. Bustamante, *Biophys. J.* **2005**, *89*, 1308-1316.

[5] E. J. G. Peterman, F. Gittes, C. F. Schmidt, *Biophys. J.* **2003**, *84*, 1308-1316.

[6] S. de Lorenzo, M. Ribezzi-Crivellari, J. R. Arias-Gonzalez, Steven B. Smith, F. Ritort, *Biophys. J.* **2015**, *108*, 2854-2864.

[7] A. Altieri, G. Bottari, F. Dehez, D. A. Leigh, J. K. Y. Wong, F. Zerbetto, *Angew. Chem. Int. Ed.* **2003**, *42*, 2296-2300.

[8] J. Gore, Z. Bryant, M. Nöllmann, M. U. Le, N. R. Cozzarelli, C. Bustamante, *Nature,* **2006**, *442*, 836-839.

[9] S. B. Smith, L. Finzi, C. Bustamante, *Science,* **1992**, *258*, 1122-1126.

[10] A. Maitra, G. Arya, *Phys. Chem. Chem. Phys.* **2011**, *13*, 1836-1842.

[11] J.-C. Chang, M. de Messieres, A. La Porta, *Phys. Rev. E,* **2013**, *87*, 012721.

[12] P. Cossio, G. Hummer, A. Szabo, *Proc. Natl. Acad. Sci. U. S. A.* **2015**, *112*, 14248-14253.

[13] A. G. T. Pyo, M. T. Woodside, *Phys. Chem. Chem. Phys.* **2019**, *21*, 24527-24534.

[14] E. Evans, *Ann. Rev. Biophys. Biomol. Struct.* **2001**, *30*, 105-128.

[15] G. I. Bell, *Science,* **1978**, *200*, 618-627.

[16] R. Merkel, P. Nassoy, A. Leung, K. Ritchie, E. Evans, *Nature,* **1999**, *397*, 50-53.

[17] E. Evans, K. Ritchie, *Biophys. J.* **1997**, *72*, 1541-1555.

[18] K. Neupane, D. A. N. Foster, D. R. Dee, H. Yu, F. Wang, M. T. Woodside, *Science,* **2016**, *352*, 239-242.

[19] T. Nicolás-García, N. Martín Sabanés, R. Bocanegra, R. D. Astumian, E. M. Pérez, B. Ibarra, *Chem,* **2025**, *11*, 102410.

[20] A. Mossa, C. Cecconi, *Eur. Biophys. J.* **2022**, *51*, 413-418.

[21] M. Manosas, J. D. Wen, P. T. X. Li, S. B. Smith, C. Bustamante, I. Tinoco, Jr., F. Ritort, *Biophys. J.* **2007**, *92*, 3010-3021.

[22] K. Neupane, D. B. Ritchie, H. Yu, D. A. N. Foster, F. Wang, M. T. Woodside, *Phys. Rev. Lett.* **2012**, *109*, 068102.

[23] K. C. Neuman, S. M. Block, *Rev. Sci. Instrum.* **2004**, *75*, 2787-2809.

[24] G. W. T. M. J. Frisch, H. B. Schlegel, G. E. Scuseria, M. A. Robb, J. R. Cheeseman, G. Scalmani, V. Barone, G. A. Petersson, H. Nakatsuji, X. Li, M. Caricato, A. Marenich, J. Bloino, B. G. Janesko, R. Gomperts, B. Mennucci, H. P. Hratchian, J. V. Ortiz, A. F. Izmaylov, J. L. Sonnenberg, D. Williams-Young, F. Ding, F. Lipparini, F. Egidi, J. Goings, B. Peng, A. Petrone, T. Henderson, D. Ranasinghe, V. G. Zakrzewski, J. Gao, N. Rega, G. Zheng, W. Liang, M. Hada, M. Ehara, K. Toyota, R. Fukuda, J. Hasegawa, M. Ishida, T. Nakajima, Y. Honda, O. Kitao, H. Nakai, T. Vreven, K. Throssell, J. A. Montgomery, Jr., J. E. Peralta, F. Ogliaro, M. Bearpark, J. J. Heyd, E. Brothers, K. N. Kudin, V. N. Staroverov, T. Keith, R. Kobayashi, J. Normand, K. Raghavachari, A. Rendell, J. C. Burant, S. S. Iyengar, J. Tomasi, M. Cossi, J. M. Millam, M. Klene, C. Adamo, R. Cammi, J. W. Ochterski, R. L. Martin, K. Morokuma, O. Farkas, J. B. Foresman, and D. J. Fox, in *Gaussian, Inc., Wallingford CT, 2016.*